University Hospital Ulm
Department of Internal Medicine II
Head: Prof. Dr. med. Wolfgang Rottbauer

Applicability of three-dimensional ultra-short echo time magnetic resonance imaging for in vivo assessment of caries lesions and early demineralization

Dissertation
Submitted to the
Medical Faculty of the University of Ulm
for the degree of Doctor of Dental Medicine

Christian Hofmann
Garmisch-Partenkirchen
2013

Dean of the Faculty of Medicine: Prof. Dr. Thomas Wirth

1st Reviewer: Prof. Dr. Volker Rasche

2nd Reviewer: Prof. Dr. Margrit-Ann Geibel

Day of grant of Doctorate: 8 May 2014

For me and my family

Table of contents

Abbreviations..... II

1 Introduction..... 1

2 Materials and methods..... 10

2.1 Ultra-short echo time MR Imaging..... 10

2.2 Feasibility study..... 11

2.2.1 Conclusion from feasibility study..... 14

2.3 Clinical study..... 16

2.3.1 Patients..... 16

2.3.2 Imaging protocol..... 17

2.3.3 Dental treatment..... 19

2.3.4 Data analysis..... 19

2.3.5 Statistical analysis..... 21

3 Results..... 22

4 Discussion..... 34

5 Summary..... 39

6 References..... 41

7 Acknowledgements..... 49

8 Curriculum Vitae 50

Abbreviations

ALARA	As Low As Reasonably Achievable
A	area
CT	computer tomography
CBCT	cone-beam computed tomography
CNR	contrast-to-noise ratio
d	lesion depth
dpulp	minimal distance between lesion and pulp
DVT	digital volume tomography
e.g.	exempli gratia (for example)
FDI	World Dental Federation
FFE	gradient echo
FID	free induction decay
FOTI	fiber-optic-transillumination
FOV	field of view
GE	gradient echo
HR	high resolution
h	height
k-space	2D or 3D Fourier transform of the MR image measured
MPR	multi planar reformatted
MS	multi-slice
MR	magnetic resonance

MRI	magnetic resonance imaging
NMR	nuclear magnetic resonance
OPG	orthopantomogram
RF	resonance/radio frequency
ROI	regions of interest
SE	spin echo
SNR	signal-to-noise ratio
SWIFT	sweep imaging with Fourier transformation
T	Tesla
TE	echo time
3D	three-dimensional
T1	longitudinal (spin-lattice) relaxation time
TR	repetition time
TSE	turbo spin-echo
T2	transverse (spin-spin) relaxation time
T2*	transverse relaxation time under consideration of local field inhomogeneities
UTE	ultra-short echo time
w	width
XR	X-ray

1 Introduction

As shown in the fourth epidemiological study on oral health conducted by the Institute of German Dentists, caries remains a widespread disease, even though a gradual decline of the prevalence of caries can be seen throughout all age groups in Germany. However, it must be noted that the caries experience regarding its distribution has changed and an increase in polarization can be observed. Amongst teenagers for instance, 79.2% of caries lesions were discovered in 26.8% of all examined [41]. This trend is also reflected in the appearance of dental decay. For quite some time, early, non-cavitated lesions clearly exceed the number of established lesions and filled cavities respectively [20]. Weerheijm et al. reported that the detection and the assessment of caries lesions, particularly with regard to the lateral tooth area, have become considerably more difficult [72].

The major component of a tooth is built up of dentin that takes up the main body of the crown, the neck and the root. It is coated by enamel in the area of the crown and by cementum in the area of the root. The inner cavity of a tooth is filled with pulp, a richly vascular soft tissue, consisting of nerves and blood vessels and supplying the outer hard tissues. The dentin can be seen as a hard tissue similar to the bone which is made up of an organic fraction (amount of 20%), an anorganic fraction (amount of 69%) and water (amount of 11%). Collagen fibers form about 90% of the total organic material of the dentin, whereas the embedded micro-crystals mainly consist of hydroxylapatite. These minerals give the dentin a greater rigidity than the bone. The hardest substance of the body is the enamel, it is cell-free and consists almost exclusively of apatite crystals (amount of 95%) which are embedded in an organic matrix (amount of 3-4%) [58].

Caries is described as an acid turnout by bacteria, a by-product of the metabolism of carbohydrate, which results in a drop in pH at the tooth surface. In response, calcium and phosphate ions diffuse out, resulting in demineralization of the tooth's hard tissues, enamel and dentin. Accountable for the production of acid is the dental plaque, a biofilm adhesive to the tooth and formed by various bacteria of which some are more caries-pathogenic than others, depending on a high substrate availability of sugars [32]. If the demineralising effects remain untreated, caries results in cavitation of the tooth

accompanied by a massive invasion of bacteria. A much more rapid progression in the inner layer of the tooth due to the higher percentage of organic material and an impairment of the pulp will be seen. The dissolving of anorganic hydroxylapatite by the use of microbially produced acids and the decomposition of organic dentin matrix through microbially produced proteolytic enzymes result in complete loss of the dental/mineral structures.

In the very beginning of lesion formation, changes in the enamel are clinically visible as white-spot lesions due to an increase in porosity. This so-called subsurface demineralization becomes more and more obvious until the four classic zones of the white-spot lesion can be identified pathohistologically. These zones are the surface zone, the body of the lesion, the dark zone and the translucent zone [40]. After cavitation of the enamel surface, the underlying structures are directly exposed to the bacterial biomass and the dentin becomes increasingly affected. The caries process can now be divided into different specific areas: the zone of necrosis (outer layer), followed by the zone of bacterial penetration and the zone of demineralization. In addition to further adjacent areas extending inwards, the zone of demineralization is the most relevant one for dental treatment [64].

The Science Committee of the World Dental Federation, FDI, has developed a new caries classification system over the past few years that is been approved by the FDI general assembly in 2011. Primarily for research, but also for use in everyday practice it shall provide assistance with caries diagnosis. Depending on the application this new matrix makes use of the well-established caries classification (yes/no) or more sophisticated sub-divisions like enamel or dentin caries with and without cavitation. These various methods for grading are meant to enable an earlier diagnosis of caries both to draw conclusions on the likely effectiveness of prophylaxis and to award better care to patients [53].

The concept of minimal intervention dentistry has evolved as a consequence of our increased understanding of the caries process and the development of adhesive restorative materials. It is now recognized that demineralized but non-cavitated enamel and dentin lesions can be 'healed' [66]. Therefore early and accurate diagnosis of caries is essential for clinicians, who require exact knowledge of the depth of caries in order to determine the appropriate type of restoration and treatment planning [48].

Today's diagnostics of caries lesions consist of the combination of clinical inspection and additional techniques. A sole visual inspection comes to a sensitivity of 12% for the detection of teeth infected by dentin caries without cavitation. Even adjuvants like dental probes or surgical loupes can only raise this value to 14% and 20% respectively [36].

In dental radiology, the use of conventional single-tooth and bitewing radiographs and orthopantomograms (OPG) is an accepted standard since the mid-1970s [42]. Dental radiographs are usually acquired and serve as valuable diagnostic aids in specific situations. However, the diagnostic benefit must be constantly balanced against the risks associated with exposure to X-ray (XR) radiation. The objective to display complex structures of the facial skull with high geometrical accuracy is limited by the projective approach causing a superposition of all structures along the ray [23]. The projective 2D representation of caries lesions, which represent 3D structures in reality, might lead to loss of valuable information and may provide insufficient details important for treatment. The main limitations inherent in conventional radiography are distortions, image blurring and overlay effects caused by the projection. The radiographic appearance of an object can change dramatically as a function of the chosen projection geometry. The proximal surfaces in the posterior region can interfere with each other to an extent that accurate and meaningful evaluation is no longer possible. In addition the correct patient positioning and its exact reproduction may be difficult to achieve. In that respect, the clinician’s skills contribute significantly to providing good quality imaging [11].

Nowadays bite-wing examination is a standard procedure for the detection of proximal caries [51]. However, non-cavitated lesions may not initially be detected precisely due to the relatively low amount of mineral loss which results in low image contrast. These lesions enlarge slowly and are not visible on radiographs until they spread beyond the inner half of the enamel [71]. In general, it can be said that initial occlusal processes within the enamel cannot be detected radiographically and that their radiographic evidence is significantly associated with heavily infected dentin [55]. Lussi reported a sensitivity of 79% for cavitated occlusal lesions using bite-wing radiography, whereas the sensitivity for lesions without any macroscopic carious cavitation was dramatically reduced to 45% [38].

The following system of classification is currently applied for the assessment of bite-wing radiographs:

C0= no proximal caries

C1= radiolucency in the outer half of the enamel

C2= radiolucency up to the inner half of the enamel

C3= radiolucency up to the outer half of the dentin

C4= radiolucency up to the inner half of the dentin

Sometimes the abbreviation D (decayed) is used instead of the abbreviation C (caries) [32].

Other devices for caries diagnosis are based on optical diagnostic methods. The DIAGNOdent unit uses laser fluorescence spectroscopy and can detect caries on occlusal and smooth tooth surfaces according to the manufacturer KaVo (Biberach, Germany). When excited by light of the appropriate wavelength, areas of carious change show an increased fluorescence in the infra-red range, which can be identified with the system. According to a study, this technique reaches significantly high sensitivity and specificity values of more than 80%, as yet only for occlusal lesions [35]. Other authors were doubtful about the procedure since it can only provide limited quantitative values. The surface properties of a tooth are not directly addressed, but an assessment of depth extension is possible [18]. Another difficulty is that bacteria produced fluorescent metabolites, which can be found not only in caries lesions but also in dental plaque and calculus, can lead to false positive test results [13]. McComb et al. actually drew the conclusion that clinical inspection was superior to the DIAGNOdent procedure and that it should be employed in combination with other procedures rather than as the sole criteria for a decision on further invasive proceedings [63].

Further diagnostic tools include fiber-optic-transillumination (FOTI). By applying a high intensity white light, which has a light-scattering effect on enamel and dentin when shone through them, caries lesions are depicted as dark areas and the loss in intensity of the light is assessed by the device. Due to the method described, the system seems most

suitable for the examination of proximal surfaces [44], where the diagnostic success may be limited by a bad inter-observer reproducibility. On the basis of a study, it was concluded that the FOTI technology, compared to direct visual and bite-wing radiographic examination, was the least reliable of the three diagnostic methods tested and that it was clearly inferior to radiography in terms of sensitivity [22].

A further possibility for detecting occlusal caries is the use of an electrical resistance monitor (ECM; LODE, Groningen, The Netherlands). The method of measuring electric impedance is based on the physical properties of enamel, which is a very good electric insulator. Demineralization leads to porosities within the enamel, which reduce insulation through water uptake. With the help of the device quantitative measured values with high reproducibility and high sensitivity and specificity values for the diagnosis of dentin caries have been reported [37]. However, the rather high value (0.23) of false-positive ratings, as shown in a different study, might lead to a substantial number of sound teeth being restored unnecessarily, which clearly limits the application of this method as sole diagnostic tool [54].

With the digital volume tomography (DVT) a new radiographic technology was introduced to dental and oral medicine in 1997, which for the first time allowed volumetric tomographic imaging similar to conventional computer tomography (CT). Techniques that allow a three-dimensional detection of anatomic structures and afterwards decompose the investigated object into a set of two dimensional layers or get a three-dimensional reconstruction of it are expected to provide the best information. By using a cone beam (cone-beam computed tomography, CBCT) it was made possible to radiate and register the whole region of investigation, the facial skull in particular, in one single rotation around the head [42]. In comparison with the conventional computer tomography, this method is less extensive and leads to a reduction of the effective radiation dose by compromising image quality. Multi-slice CT shows the highest exposure values, while CBCT systems range between CT and conventional radiography [60]. For proximal lesions a sensitivity of 80% and a specificity of 96% were reported for CBCT, while using bite-wing radiographs only 29% of lesions with cavitation could be identified correctly [19]. However, the image quality in CBCT can be impaired by beam-hardening artifacts as well as motion artifacts. Further studies indicated that CBCT images did not necessarily

enhance detection of proximal caries in comparison with periapical images [71]. In addition one study even concluded that no difference in sensitivity (0.175) or specificity (0.573) could be shown between the two modalities [52]. In principle, it is possible to detect carious lesions with CBCT, since changes in density caused by mineral extraction are captured. Nevertheless, this radiographic technique does have limitations as well. Besides a higher effective dose of radiation for the patient, false-positive results due to technical artifacts caused by adjacent metallic restoration materials or implants are likely [42].

CBCT cannot serve as the sole imaging modality adopted for every eventuality, as the ALARA-principle, according to which radiation exposures must be kept "As Low As Reasonably Achievable", constitutes a fundamental guideline of radiation protection and safeguards. When dealing with X-rays the reduction of the radiation exposure is mandatory and the patient's exposure to X-rays must be kept as small as possible and as large as necessary [6, 7]. In accordance with § 23 of the Radiation Protection Act, an X-ray examination can only be taken when a specific indication can be justified and only if it is shown that the benefits to human health outweigh the radiological risk. Another key point in the legislative texts is the fact that other techniques with a comparable beneficial effect for health, with little or no radiation exposure have to be taken into account [8]. In 2012 the European Commission issued a guideline stating that even though cone-beam computed tomography (CBCT) may provide the required tomographic information its application in caries detection and diagnosis is not indicated due to the related high X-ray dose and strong artifacts caused by metal [12, 61]. It appears that CBCT will remain reserved for other special fields like oral and maxillo-facial surgery or orthodontics, in which it has virtually become indispensable [42]. A recently published study reported that the exposure to dental X-rays performed in the past is associated with an increased risk of intracranial meningioma. Although X-ray dose has decreased in the meanwhile, this study clearly indicates the need for alternative imaging methods in dental diagnostics [10].

Magnetic resonance imaging (MRI) has proven excellent clinical performance, especially in the assessment of soft tissue structures and has become one of the mainstay imaging tools in diagnostic radiology. The X-ray free versatile three-dimensional assessment of morphology and function raised the interest of MRI as a generic imaging tool in dental

applications already in 1981 [24, 56]. It has been proven that the application of MRI for imaging the teeth and the periapical region provides useful information on non-mineralized structures, which are not readily accessible by the established XR-based imaging methods [65]. Typical applications of MRI include the assessment of extracranial tumors [29, 65], the assessment of the morphology and function of the temporomandibular joint [9, 21, 39, 47, 62, 70], the planning of dental implantation procedures [1, 15, 16, 27, 45], and the assessment of impacted teeth [67].

The nuclear magnetic resonance (NMR) phenomenon is based on the interaction between radio waves and hydrogen nuclei in the presence of a static magnetic field. Since the hydrogen nucleus, in the human body naturally occurring as water (H20), is a single positively charged proton and since it possesses the property to spin, it generates a small magnetic field and therefore produces an NMR signal. When magnetized, the nucleus responds to exposure to radio-waves at a particular frequency and interacts with an alternating magnetic field of a specific resonance frequency (RF) by sending back a radio-wave signal called a "spin echo". The spin echo signal is made up of multiple frequencies, reflecting different positions along the magnetic field gradient. Furthermore spatially varying magnetic fields (gradients) allow us to spatially encode the nuclei and to construct tomographic images.

The magnetization is a vector quantity that can be depicted by a longitudinal component along the so-called z-axis representing the main magnetic field and by a second component perpendicular to the first called the transverse magnetization, which is in the xy-plane. Only transverse magnetization, which can be generated by rotation of the magnetization vector by a high-frequency pulse produces signal. The time for a proton to become magnetized in a magnetic field or alternatively the time required to regain longitudinal magnetization following an RF pulse, is the longitudinal (spin-lattice) relaxation time T1. The transverse (spin-spin) relaxation time T2 is a measure of how long transverse magnetization would last in a perfectly uniform external magnetic field and hence indirectly indicates the maximal time available for signal reception. Depending on tissue type, the protons of water molecules have different relaxation properties. These relaxation properties and the proton concentration contribute significantly to the transverse magnetization at the time of signal acquisition. By varying the repetition time

(TR) and echo time (TE) parameters, the transverse magnetization can be varied for optimization of specific image contrast.

The main limitation for MRI to identify caries lesions is its inability to assess hard tissues and to only poorly delineate the mineralized structures of the tooth. The high mineral content of these structures causes an extremely low concentration of free protons which leads to only weak magnetization and a random dephasing at the susceptibility interfaces in the mineral structures, which results in a spin–spin relaxation time of less than 1ms for dentin [59] and of less than 250µs for enamel [14], both values measured at 1Tesla (T) main magnetic field strength. With these short T2 values for enamel and dentin, it was not possible to detect any signal from dental structures using conventional sequences on previous scanners.

Numerous approaches to direct imaging of the mineralized structures by MRI have been published, including in vitro approaches such as solid-state imaging techniques [2], multinuclear approaches [74], single point imaging techniques [17], sweep imaging with Fourier transformation (SWIFT) [25, 26], and ultra-short echo time (UTE) imaging [24, 57]. Even though all studies revealed the potential of MRI for the assessment of the hard tissue components of the teeth, the related long acquisition times or the required high field strengths have so far omitted to transfer the obtained results to in vivo applications. As an alternative to the direct visualization, indirect methods in which the teeth were embedded in a dedicated signal providing material have been investigated [33, 34, 46, 73]. Since direct visualization of the short T2 tissues was not required, conventional (multi) spin echo techniques were applied. In vitro [33, 34, 73] as well as in vivo [46, 68] evaluation could prove a substantial signal enhancement of the caries lesions, which was attributed to protons penetrating into the lesion through the porous demineralized tooth substance. Additional problems are caused by artifacts introduced by dental filling materials that have so far restricted the wider application of MRI in dentistry. However, it could be shown by Boujraf in an initial feasability study that the artifact level in dental MRI highly depends on the imaging method used and also on the composition of the dental materials [4].

Since nowadays UTE sequences have been established on clinical scanners, it is the objective of this thesis to demonstrate the applicability of three-dimensional ultra-short echo time (3D-UTE) imaging for in vivo assessment of caries lesions and early demineralization stages.

2 Methods and Materials

2.1 Ultra-short echo time MR Imaging

For approaching short echo times, gradient echo imaging techniques are usually applied (Figure 1a). The limiting factor for the echo time is the required slice re-phasing (s), the phase encoding (p), and the pre-phasing gradient (m) in read direction. The required gradient waveforms cause a substantial gap between the center of the excitation pulse (green line in Figure 1a) and the minimal possible TE (start of red bar in Figure 1a). For further reduction of TE, in this thesis a dedicated imaging method [24] was applied and compared to the conventional imaging approaches. The dedicated 3D-UTE technique (Figure 1b) comprises non-slice selective volume excitation thus avoiding the need for any slice re-phasing. The non-slice selective excitation is combined with a radial free-induction decay readout avoiding any pre-phasing or phase encoding gradients. Doing so enables a substantial reduction of the possible echo time, which is only limited by the time required for switching the frontend between transmit and receive mode. For the whole-body scanner (Achiva 3.0T, Philips Healthcare, Best, the Netherlands) applied in this study, the minimal TE possible was as 50µs.

For comparison of the performance of the UTE approach, data was also acquired by means of conventional spin-echo and gradient echo techniques [3].

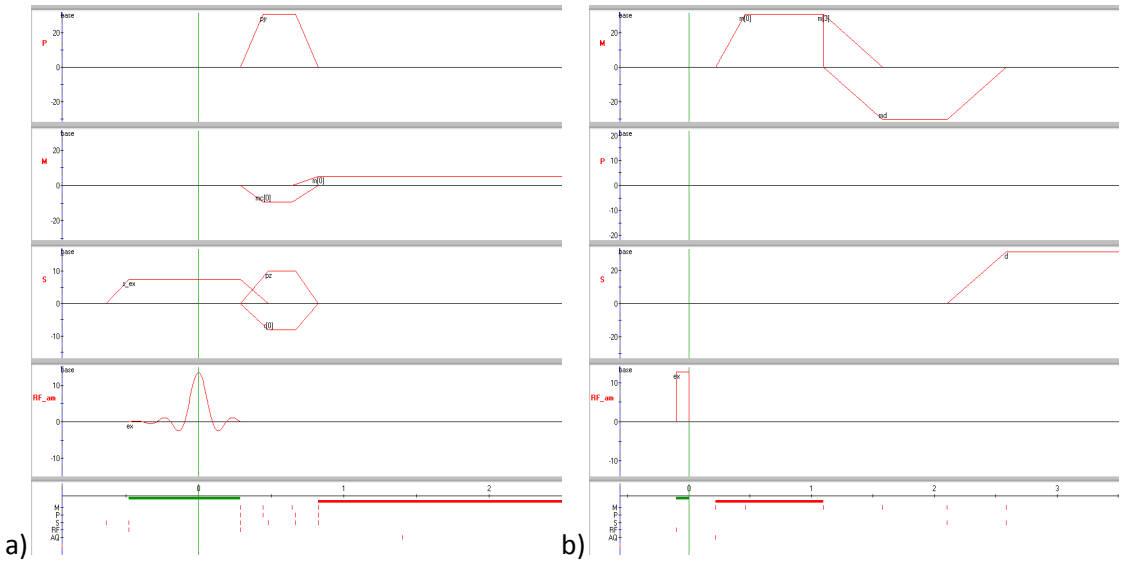


Figure 1: MR sequence diagram of (a) a conventional short TE gradient echo technique in comparison to (b) a dedicated ultra-short TE FID technique.

2.2 Feasibility study

The application of MRI as an imaging modality for dental diagnosis has not entered clinical routine due to its limited performance in the assessment of mineralized hard tissues. As explained above, these structures, especially the outer layer of the tooth, the enamel, show only a low concentration of free protons and therefore cause only weak magnetization. Conventional magnetic resonance imaging (MRI) sequences show only a very limited performance in delineation of the mineralized components and are not able to detect them due to the related very short T2/T2* – relaxation properties of well below 1ms for dentin [59] and of less than 250µs for enamel [14]. With the recently introduced ultra-short echo time (UTE) MRI techniques, image acquisitions with echo times as low as a few µs became possible, whilst switching times in the order of 50µs can be realized on the MR system utilized in this thesis.

Since the application of the 3D-UTE has not been proven for direct visualization of dental hard tissues, a pre-study was performed in extracted human teeth. In this pre-study the 3D-UTE technique was optimized for the assessment of the tooth morphology in vitro. The goal was to demonstrate the feasibility of UTE imaging for assessing the tooth tissue components including enamel, dentin and pulp.

Preparation of samples:

72 extracted human teeth were stored in formalin solution. The samples included incisors, canines, pre-molars and molars. Since teeth in the oral cavity are physiologically surrounded by constant moisture of saliva, all teeth were put into little glas tubes and embedded in agarose gel to mimic the biological conditions and to minimize possible susceptibility artifacts at the air-tooth interface.

MRI Measurement:

All MR imaging was performed on a clinical 3Tesla whole body MRI system (Achieva, Philips Medical, Best, Netherlands) and the data was acquired with a single element (65x50mm) of a two times two channel prototype carotid coil (Philips Research Europe, Hamburg, Germany).

For assessment of the performance of the 3D-UTE technique in direct comparison with the conventional imaging techniques, each tooth underwent 5 different scans with different echo times (TE) and different volumetric imaging techniques, comprising:

- 3D-gradient echo (3D-FFE)
- 3D- spin echo (3D-SE)
- 3D-free induction decay (3D- UTE)

During the subsequently acquired scans, the sample was not moved to ensure proper registration of the images for subsequent data analysis. Relevant image acquisition parameters for the different techniques are provided in Table 1. Since in 3D-UTE a different acquisitions scheme (radial k-space coverage vs. Cartesian coverage in conventional imaging) is used, differences between the different investigated techniques can either be caused by the shorter TE or eventually by the modified acquisition scheme. To rule out any impact from the acquisition scheme, in 3D-UTE additional acquisitions were performed with longer echo times similar to the 3D-FFE techniques.

Table 1: Acquisition parameters for the different investigated imaging techniques

FOV [mm³]	TR [ms]	TE [ms]	NSA	Resolution [mm³]	Flip Angle [°]	MR technique
80	9.4	0.05/2/4	3	0.2x0.2x0.2	10	3D-UTE
80	164	14.6	1	0.2x0.2x0.2	90	3D-SE
80	12.8	4	3	0.2x0.2x0.2	10	3D-FFE

The optimization of the 3D-UTE sequence included the accurate assessment of the delays of each individual gradient channel as well as the UTE acquisition parameters including the excitation flip angle, readout bandwidth, and the number of radial encodings. From the gradient channel delays, a mean eddy-current decay constant was derived. During reconstruction, the distorted trajectory was approximated by convolution of the ideal 3D radial trajectory with a mono-exponential decay function [3].

Data analysis:

For comparison of the different techniques, regions of interest (ROI) were manually drawn in each investigated tooth. A single ROI was identified in enamel, dentin, pulp, background and the agarose in each tooth. For identification of the ROI, the 3D-UTE image with minimal echo time was used. All ROIs were then transferred to the images acquired with the other techniques. The resulting images were compared according to the signal-to-noise ratio (SNR) and contrast-to-noise ratio (CNR). SNR was calculated as $SNR\ (I) = \frac{S_I - S_{BG}}{\sigma_{BG}}$, with S_I and S_{BG} being the mean intensities of the respective structure I and the background, and σ_{BG} being the standart deviation of the background. CNR was calculated as $CNR\ (1,2) = \frac{S_1 - S_2}{\sigma_{BG}}$, with S_1 and S_2 being the respective mean intensities of the respective structures. The significance of any differences was quantified by a two-tailed paired Student's t-test with a two-sample equal (homoscedastic) variance. P-values below 0.5 were considered significant.

2.2.1 Conclusion from feasibility study

Figure 2 exemplarily shows a single slice extracted from the 3D data set of an incisor acquired with the acquisition techniques as described in Table 1. The images in the bottom row represent a simple inversion of the images to generate an XR-like appearance of the images. As expected, the 3D-UTE image acquired at an echo time of TE = 4ms shows very similar image contrast as the respective 3D-FFE image acquired with a similar echo time. From the images it can be appreciated that only for the 3D-UTE acquisition with minimal echo time, a clear delineation between the different dental tissues, especially between the enamel and the dentin, can be achieved. The quantitative assessment of mean image intensities of the major tooth components clearly proves the qualitative findings in Figure 3. The mean differences in image intensities between enamel-dentin, enamel-noise and dentin-pulp are shown. All differences resulted as highly significant with p-values below 0,001.

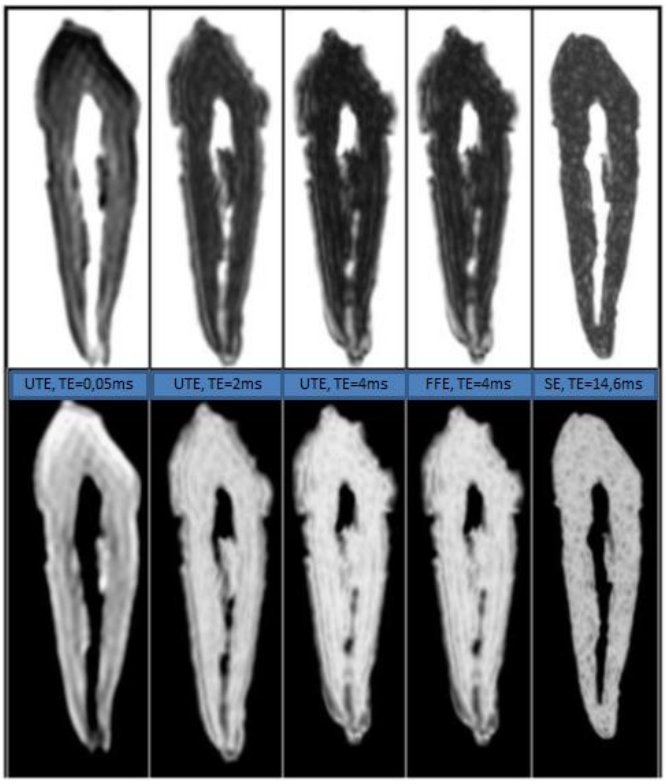


Figure 2: Images of the same slice at different TEs with different acquisition approaches. The images in the 2nd row are inverted images of those shown above.

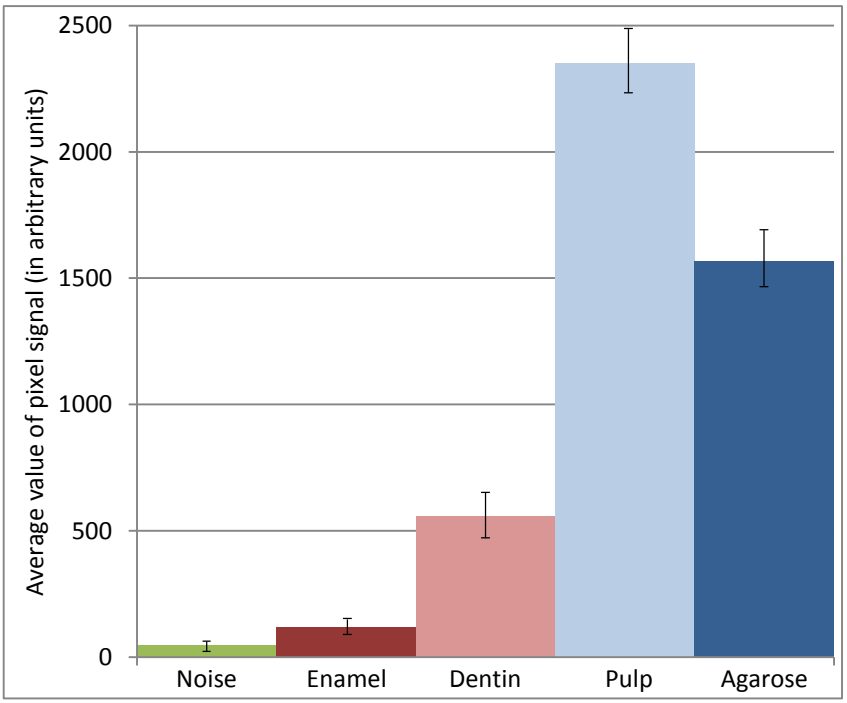


Figure 3: The average value of pixel signal in different dental tissue components compared to noise and agarose (in arbitrary units). The standard deviation is included as a black line in every column.

Precedent research from other authors has shown that the T2 values of enamel and dentin are less than 1ms for dentin [55] and less than 250µs for enamel [14], both values measured at a 1 Tesla MRI system. Therefore it is not possible to detect sufficient signal from these structures using conventional sequences even with minimized echo times (TE). In this in-vitro feasibility study, we could show that high-resolution MRI with ultra-short echo times (UTE) enables the assessment and delineation of the different hard dental tissues. With the current acquisition parameters, direct transfer to in vivo applications appears critical due to the still very long acquisition times in the order of 30 minutes. Since the final goal for dental MRI would be the identification of early caries lesions, direct visualization of the enamel and dentin might not finally be required and it might be sufficient to visualize local acid accumulations as initial markers for initial carious degradation of the related enamel and dentin layers. The initial local acid accumulation will cause a local increase in proton density with related increase in local magnetization. But since the mineral structure will still be intact, the local T2/T2* properties will not change. Due to the increased magnetization, however, more rapid acquisitions, e.g. using a single signal average only in combination with coarser spatial resolution, may be sufficient for identification of the initial carious lesions and demineralizations.

We have proven in-vitro that ultra-short echo time (UTE) MR imaging is capable of delineating the different hard tissues of teeth at high spatial resolution and sufficient contrast. Transfer to in vivo applications appears promising with respective adjusted imaging parameters. Whether the resulting sensitivity will be sufficiently high has to be proven in further studies.

2.3 Clinical study

In a cohort of 40 patients, the proposed UTE technique was evaluated and compared with conventional spin echo MRI and bitewing X-ray. The image protocol was approved by the local ethics committee of the University of Ulm (Application-No. 221/08: Applikation der Magnetresonanztomographie für zahnmedizinische Fragestellungen) and written informed consent was obtained from all patients prior to the dental MRI examination.

2.3.1 Patients

Forty patients (16 female, 24 male, mean age 41 ± 15 years), which were acquired from the clinical students' course of the University of Ulm, were enrolled in this clinical study. The patients were randomly selected and showed various states of tooth decay. Prior to the MR examination all patients underwent clinical examination including visual assessment of the teeth and bitewing X-ray examination of either side of the jaw. All XR data was acquired with a digital intra-oral detector (Sidexis, Sirona Dental Systems, Bensheim) at a spatial resolution of $39^2 \mu m^2$. Clinical examination and X-ray examination revealed a variety of restoration materials in the patients: gold (n=3), cement (n=23), amalgam (n=104) and composite (n=262) fillings and gold (n=71) and ceramic (n=6) crowns.

The MR examination was accomplished within 14 days after the initial investigation before any dental treatment of the lesions was carried out. Patients with wires and fixed braces (e.g. multi-band technique or retainers) used for orthodontic treatment were excluded due to the expected severe image artifacts caused by the nickel or cobalt containing alloys.

2.3.2 Imaging protocol

All MR imaging was performed on a clinical 3Tesla whole body MRI system (Achieva, Philips Medical, Best, Netherlands) and the data was acquired with a single element (65x50mm) of a two times two channel prototype carotid coil (Philips Research Europe, Hamburg, Germany, Figure 4a) equipped with gradient hardware capable of maximum gradient amplitude of 40 mT/m using a maximum slew rate of 200 mT/ms. The coil was placed at the respective side of the jaw and then affixed with a Vac-Lok neck cushion (Medtec, USA). Sandbags were placed on the left and right side of the head to avoid patient motion during the examination (Figure 4b). All patients underwent a standardized MRI protocol.



Figure 4: Prototype carotid receiver coils (a) and one patient ready to undergo the examination (b).

A fast initial survey included two orthogonal surveys and a coil-sensitivity reference scan, followed by two diagnostic scans, one multi-slice turbo spin-echo (MS-TSE) and one 3D ultra-short echo time (3D-UTE) sequence for caries lesion assessment. Each HR survey was individually planned for the left and right side. The surveys were planned along the jaw in parasagittal and transversal direction to assess the optimal position of the coil. If necessary the coil was repositioned and the scan was repeated. The coil sensitivity reference scan was later on used to homogenize the signal intensity of the images acquired by the prototype surface coil. Two-dimensional MS-TSE acquisitions with an in-plane resolution of 0.4x0.4mm and a slice thickness of 1mm and a 3D-UTE sequence with an isotropic resolution of $0.8mm^3$ were applied. A detailed overview of the MRI acquisition parameters is provided in Table 2.

Table 2: Magnetic resonance imaging (MRI) sequence parameters for the initial survey scan and the two diagnostic scans:

	High Resolution (HR) Survey	**Multi Slice - Turbo Spin-Echo (MS-TSE)**	**3D ultra-short echo time (UTE)**
Technique	Spoiled gradient echo (GE)	Turbo spin-echo	Spoiled Free Induction Decay(FID)
k-space encoding	Cartesian	Cartesian	3D radial
Excitation	slice selective	slice selective	non-slice selective
Flip angle [°]	20	90	10
resonance frequency (RF) pulse duration [ms]	3.8	4.2	0.05
Echo time [ms]	2	8.1	0.05
Repetition time [ms]	3.8	625	5
Readout time [ms]	2.5	3	0.8
# echoes	1	16	1
Acquired res. [mm³]	1.5x1.5x5	0.4x0.4x1	0.8x0.8x0.8
Reconstructed res. [mm³]	1.5x1.5x5	0.4x0.4x1	0.5x0.5x0.5
Field of view [mm³]	300x300x20	230x230x8	120x120x120
Scan time [min]	0:51	5:32	7:49

The MS-TSE sequence was included in the imaging protocol for verification of the performance of the conventional MR techniques in detection of caries lesions and early demineralization. The MS-TSE scan was planned in transversal direction along the jaw (Figure 5a). The central point of the spherical field of view (FOV) of the 3D-UTE sequence was placed between the premolars and molars in transversal direction (Figure 5b) and between the lower and upper jaw in parasagittal direction (Figure 5c).

In order to achieve an image quality only affected by the properties of the teeth tissue, no acceleration techniques like half-scan or parallel imaging were used. Since no long T2 components are superimposed to the dental tissue, no fat or long T2 suppression pre-pulses were applied to minimize acquisition time [30].

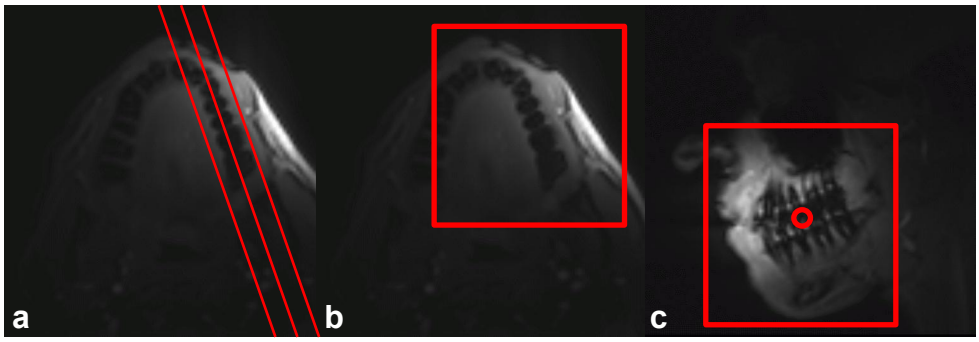


Figure 5: Planning of the TSE sequence (a) transversal along the jaw and the 3D-UTE sequence in (b) transversal and in (c) parasagittal direction.

2.3.3 Dental treatment

After the MR examination all patients underwent dental treatment in the clinical students' course of the university.

Four patients volunteered for in-situ documentation. Intra- and extra-oral pictures were taken prior to the treatment, after filling removal, after excavation and after conservative therapy. The excavation of caries was controlled by caries detector fluid (1% acid red) together with frequent manual exploration of the hardness of the dentin. To document the real extent of the lesion in-situ, a bitewing X-ray of the plaster model of the post-excavation imprint of three patients was acquired. One patient could not be evaluated as described due to a partly blurred 3D-UTE image caused by amalgam.

2.3.4 Data analysis

For analysis, all data was transferred to a medical workstation (ViewForum, Philips Healthcare). For data collection and analysis, the 3D-UTE MRI data was reconstructed at a resolution of 0.5x0.5x0.5mm³ and multi planar reformatted (MPR) along the lower jaw in a parasagittal orientation similar to the planning of the MS-TSE scans resulting in an orthopantomogram-like visualization. Both the thickness and the position of the MPR slice were adapted manually to guarantee the best possible delineation of the teeth.

The measurements in the X-ray images of the patients and of the plaster models could be directly performed.

Due to the local demineralization and the accompanying accumulation of watery fluid in the dental tissues, the proton density and the local T2/T2* are supposed to increase causing a local signal enhancement in the enamel or dentin layer. All bright spots inside a tooth not belonging to the dental pulp are defined as a caries lesion if they show a signal brighter than the mean value plus two times the standard deviation of the surrounding tooth. All MRI images were reviewed by two experienced MRI readers and a dentist in consensus.

In all image modalities height (h), width (w) and the area (A) of identified lesions as well as the minimal distance between lesion and pulp (d_{pulp}) were measured. Additionally, in the 3D-UTE images the depth (d) of a lesion was assessed (Figure 6b). For each identified lesion the signal-to-noise ratio (SNR) and the contrast-to-noise ratio (CNR) were determined. The SNR values were determined by calculation of the ratio of the mean intensity of an identified lesion and the respective standard deviation. All SNR measurements were performed after correction of the intensities for the sensitivity profiles of the surface coils. The CNR was determined by the difference between the mean intensity of the lesion and of the dentin and the respective standard deviation of the dentin.

The lesion size in the bitewing X-rays of the plaster models attained in three exemplary cases was qualitatively compared to the results of the in-vivo MR and XR images.

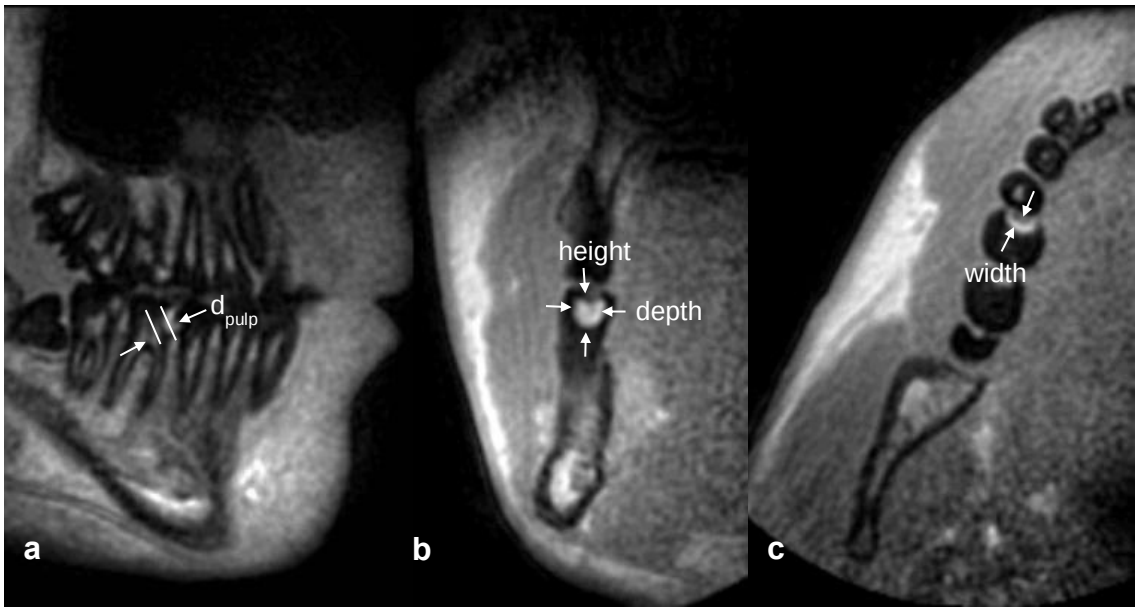


Figure 6: 3D-UTE appearance of a caries lesion in (a) parasagittal, (b) coronal and (c) transversal perspective of the teeth at the left side of the jaw with lesion extensions indicated.

2.3.5 Statistical analysis

According to their visibility in the different imaging techniques and for statistical purposes the lesions were divided into three different classes (CI, CII and CIII). Lesions of class CI are clearly visible in all three image types (XR, 3D-UTE and MS-TSE). CII lesions are clearly visible in the XR and 3D-UTE images but not visible in the MS-TSE images and CIII lesions are solely visible in 3D-UTE.

The lesion extension in two dimensions (height h, width w), the area A of the lesion and the distance d_{pulp} between the lesion and the pulp were compared between the XR, 3D-UTE and MS-TSE images.

To assess the statistical significance of the resulting differences between the investigated techniques, a two tailed paired t-test with a two-sample equal (homoscedastic) variance was used. Differences were considered significant for p values below p=0.05.

3 Results

The imaging protocol could be completed in 39 patients. One patient had to be excluded due to claustrophobia that arose while lying in the whole body MRI scanner. The dental examination could be completed in less than 45 minutes, including the setup of the patient, the repositioning of the coil between the left and the right side and the planning of the scans. The measurement procedure and the scan times in general were well tolerated by the patients.

Two patients, one provided with two osteosynthesis plates in the lateral area of the skull and one provided with 12 gold crowns and 10 amalgam fillings, had to be excluded because of severe image degradation. All other artifacts caused by dental filling materials were restricted to local distortions, which were limited to a single tooth (n = 9) or at maximum to neighboring teeth (n = 2). All in all, 14 teeth could not be analysed by either MRI imaging technique.

Due to the limited penetration depth of the surface coil and the strong decay of the coil sensitivity profile, the distance between the coil and the teeth was decisive. Some signal-to-noise (SNR) reductions could be observed in patients where the distance between the coil and the center of the first molar of the lower jaw exceeded 2.5 cm. Therefore a clear delineation between the enamel and the dentin layer could not be achieved in all patients, yet a distinguishable delineation between the pulp and the mineralized tissues could be achieved in all MRI scans. The mean signal-to-noise ratio in all lesions resulted to 6.7 ± 2.7, whereby no significant SNR differences could be observed between the different lesion categories. Likewise, the contrast-to-noise ratio (CNR) values that resulted in 16.2 ± 10.0 did not vary significantly between the three categories.

Since enamel and dental fillings appear dark in the MRI images, only a poor delineation of the occlusal surfaces can be achieved when teeth are in direct contact with their antagonists. However, when surrounded by a saliva layer (i.e. interdental spaces) or by soft tissues, like the tongue or the cheek, a clear borderline becomes visible. A successful example of a scan depicting all dental components mentioned is shown in figure 7.

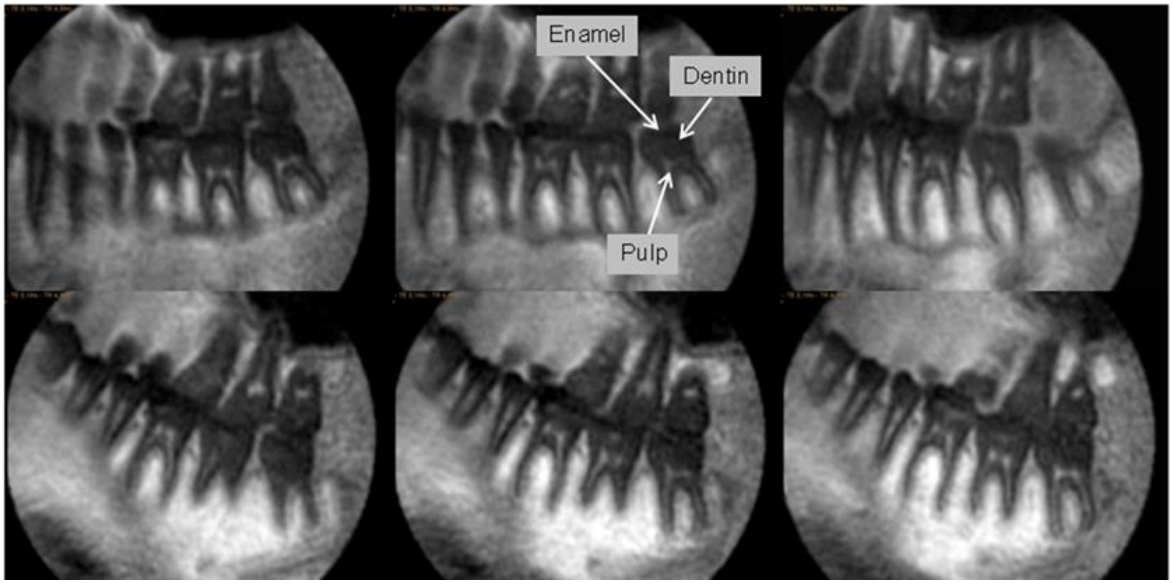


Figure 7: Illustration of a sequence of multiple slices of the same 3D-UTE dental examination. The different dental tissues (enamel, dentin and pulp) can be defined in a statistically significant manner (p-values <0.01 between enamel and dentin).

In total 157 caries lesions were identified by 3D-UTE, 137 lesions by XR, and 27 lesions by MS-TSE. In one out of the 14 teeth not accessible by MRI, a caries lesion was identified on the respective X-ray images. Furthermore 24 lesions were only identified by 3D-UTE, including secondary caries (n=6), occlusal (n=3), and initial approximal caries lesions (n=15). Overall 161 caries lesions could be identified, whereby 157 were identified by 3D-UTE and 4 additional ones could be identified by XR. The lesions were categorized as CI lesion (n=27), CII lesion (n=110) and CIII lesion (n=24).

Taken as a whole, this study enabled to obtain a sensitivity of 97.5% for 3D-UTE, 85% for X-ray and 17% for MS-TSE.

As the majority of lesions (68%) were categorized as C-II lesions, representative examples are shown in figure 8 and figure 9.

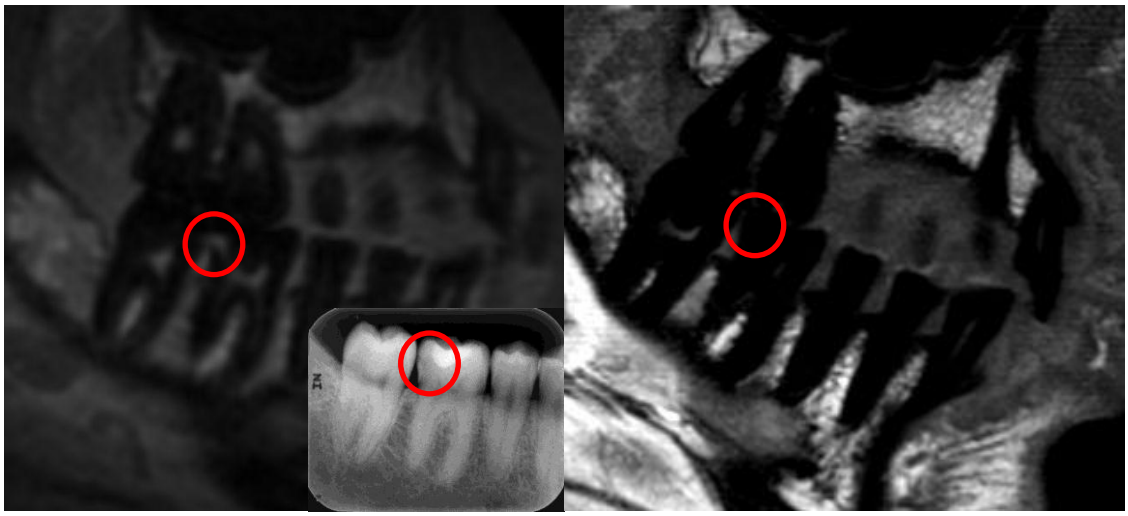


Figure 8: Appearance of an initial approximal caries lesion (circle) in UTE (left), MS-TSE (right), and the respective X-ray (inset).



Figure 9: Appearance of an occlusal caries lesion (circle) in UTE (left), MS-TSE (right), and the respective X-ray (inset).

In direct comparison all lesions appeared larger in the 3D-UTE images than in the XR (category CI and CII) or MS-TSE (category CI) images. On the contrary, the lesions in MS-TSE appeared much smaller than in the X-ray findings with less enhanced display quality. One main focus was the measurable distance between the lesion and the pulp, which differed remarkably. Many lesions, which seemed in safe distance to the pulp in the bitewing radiographs, nearly touched its border in the 3D-UTE images as shown for a hidden caries in figure 9 and an approximal caries in figure 10 (circle). The dashed circle in figure 10 shows a secondary caries lesion beneath an amalgam filling of the upper left canine detectable with 3D-UTE. In this case the XR image did not allow for an exact

diagnosis due to superimposed structures, while the 3D-UTE derived images could clearly identify even the initial lesion of the adjacent tooth.

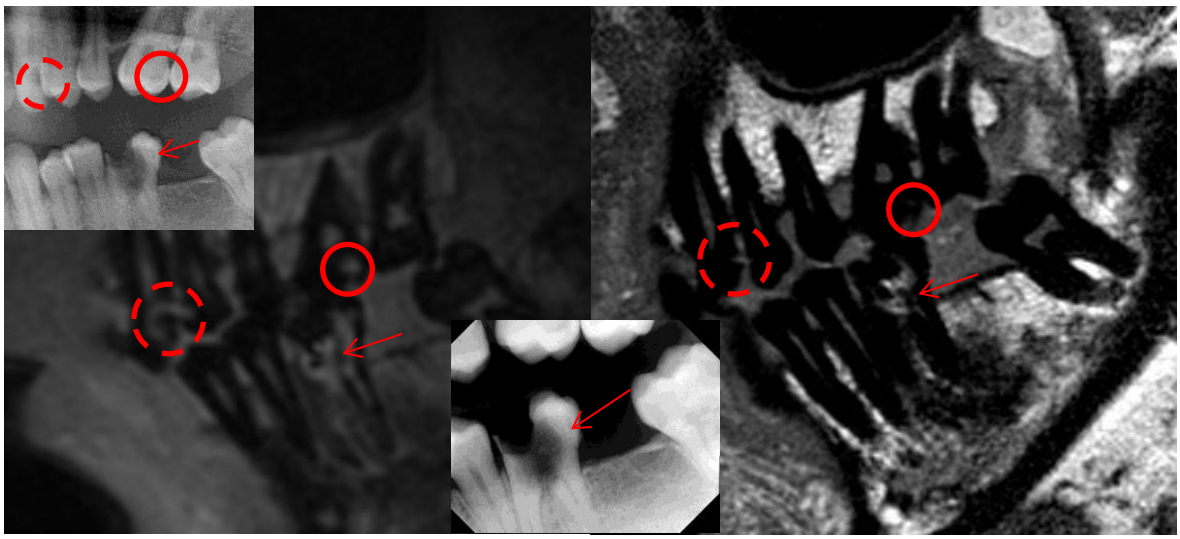


Figure 10: Appearance of an initial caries lesion (circle), a secondary caries in the proximity of an amalgam filling next to an initial lesion (dashed circle), and a massively progressed caries beneath a temporary cement filling (arrow) in 3D-UTE (left), in MS-TSE (right) and the respective X-rays (insets).

Table 3: Mean values and standard deviations of the lesion parameters [width (w), height (h), minimal distance to the pulp (d_{pulp}), area (A)] and the respective p-values of the comparison between different imaging modalities belonging to the same category. Gray shaded values are not significant.

category	**CI**						**CII**			**CIII**
	MS-TSE	**UTE**	**XR**	**$p_{MSTSE-UTE}$**	**$p_{MSTSE-XR}$**	**p_{UTE-XR}**	**UTE**	**XR**	**p_{UTE-XR}**	**UTE**
w [mm]	2.6 +/- 1.9	3.6 +/- 1.8	3.4 +/- 1.7	<0.01	<0.01	<0.05	3.0 +/- 1.8	2.5 +/- 1.8	<0.01	1.7 +/- 0.7
h [mm]	2.7 +/- 1.7	3.8 +/- 2.0	3.5 +/- 1.9	<0.01	<0.01	<0.01	2.0 +/- 0.9	1.5 +/- 0.7	<0.01	1.5 +/- 0.7
d_{pulp} [mm]	1.5 +/- 0.9	1.0 +/- 0.5	1.7 +/- 0.8	<0.01	0.22	<0.01	1.3 +/- 0.6	2.2 +/- 1.0	<0.01	1.6 +/- 0.7
A [mm²]	8.0 +/- 11.4	12.6 +/- 14.2	10.6 +/- 12.8	<0.01	<0.01	<0.01	4.4 +/- 3.1	2.7 +/- 2.1	<0.01	2.1 +/- 1.2

The quantitative analysis of the geometrical properties of the lesions and the respective statistical significance for all three imaging approaches and lesion categories are summarized in table 3.

In category CI, the evaluated information for all lesions detected by MS-TSE showed significantly smaller values for all measurable parameters (Figure 11a). Compared to the 3D-UTE and XR results, the parameters width (w), height (h) and area (A) were all significantly smaller ($p < 0.01$ for all three indexes), whereby the comparison between 3D-UTE and X-ray provided significantly higher values in all respects in the favor of the UTE-images. By implication, values for the parameter d_{pulp} resulted in significantly smaller values in the UTE-images, whereby for this parameter no significant differences could be observed between the MS-TSE and XR images (grey shaded p-value = 0.22 in table 3).

In category CII, all resulting values of the 3D-UTE images were significantly higher than the ones of the X-ray images, except for the distance to the pulp (d_{pulp}) of course which resulted in significantly lower values (Figure 11b).

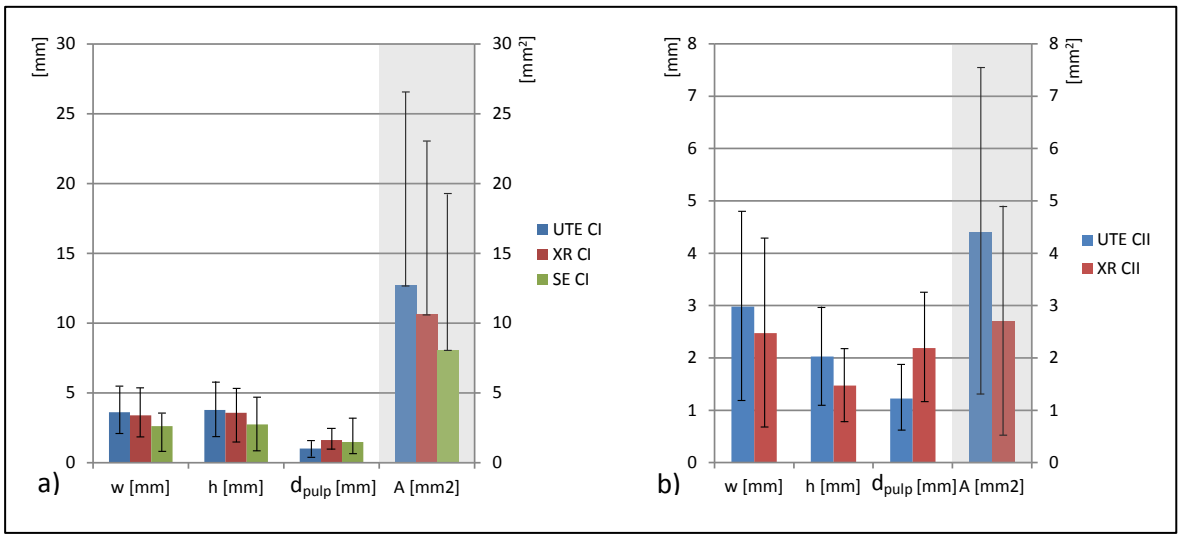


Figure 11: Column diagrams of lesion extensions of the different lesion parameters [width (w), height (h), minimal distance to the pulp (d_{pulp}), area (A)]. a) Comparison within category CI referring to the different imaging techniques 3D-UTE (UTE CI), X-Ray (XR CI) and MS-TSE (SE CI). b) Comparison within category CII referring to the imaging techniques 3D-UTE (UTE CII) and X-Ray (XR CII). The standard deviation is included as a black line in every column and for reasons of clarity the negative lines of the standard deviations of the area (A) are omitted in a).

In an inter-class comparison all lesions visible in 3D-UTE were evaluated. All geometrical properties available, the distance d_{pulp}, the lesion extension in all spatial directions (width, depth and height) and the area were compared (Figure 12). CIII lesions were smallest and show smaller lesion extensions compared to CI and CII lesions. Differences in lesion size between CI and CIII as well as between CII and CIII were significant in all three spatial directions. However, comparing the lesion size of CI and CII lesions, the differences seemingly became smaller and the parameters width and distance d_{pulp} became either no longer significantly diverse ($p = 0.1$) or just showed a trend to lower values ($p = 0.09$).

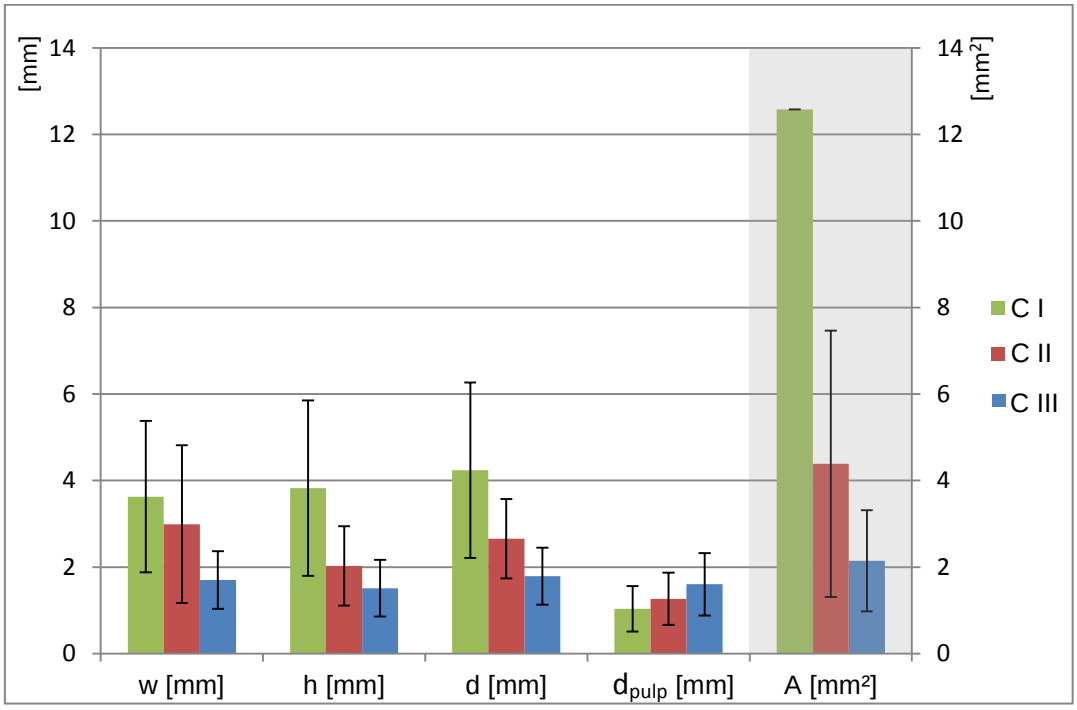


Figure 12: Column diagram of the inter-class comparison of the different lesion categories CI, CII and CIII. All geometrical properties [width (w), height (h), depth (d), minimal distance to the pulp (d_{pul}), area (A)] of all lesions detectable with the 3D-UTE technique are represented in this figure. The black line within each column represents the standard deviation and for the parameter area (A) of category CI the standard deviation (value +/- 14.2) is omitted in the visualization. The labelling [mm²] of the Y-axis on the right only refers to the gray shaded column of the parameter area (A).

Table 4: Statistical significances between the different lesion categories (p_{CI-CII}, $p_{CI-CIII}$, $p_{CII-CIII}$) obtained in figure 12 for all geometrical properties [width (w), height (h), depth (d), minimal distance to the pulp (d_{pulp}), area (A)].

	w	**h**	**d**	**d_{pulp}**	**A**
p_{CI-CII}	0.1	<0.01	<0.01	0.09	<0.01
$p_{CI-CIII}$	<0.01	<0.01	<0.01	<0.01	<0.01
$p_{CII-CIII}$	<0.01	<0.05	<0.01	<0.05	<0.01

Treatment cases

The in-situ documentation includes examples for each category (CI-, CII- and CIII-lesions). Four patients underwent a showcase treatment in which intra-oral pictures were taken prior as well as during the session. Secondly, silicone-based impressions of the lesions were taken after caries excavation for further quantitative analysis.

Case 1

The first case presents a second upper molar deeply damaged by caries. Clinical visual inspection combined with the XR examination revealed large defects from both the disto-buccal and the mesio-approximal region. Especially the disto-buccal defect seemed so large that endodontical treatment had to be taken into consideration. However, the transversal slices of the 3D-UTE data sets indicated a sufficient distance between the lesion and the pulp which indeed could be maintained after caries excavation and the tooth in question could be restored with composite filling materials (Figure 13e). The respective intra-oral pictures, the MR and X-ray images are all shown in figure 13, whereby the lesions are labeled with white arrows in the MR images and with black arrows in the X-ray images. As expected the lesion sizes in the MS-TSE images appear much smaller than in the 3D-UTE images.

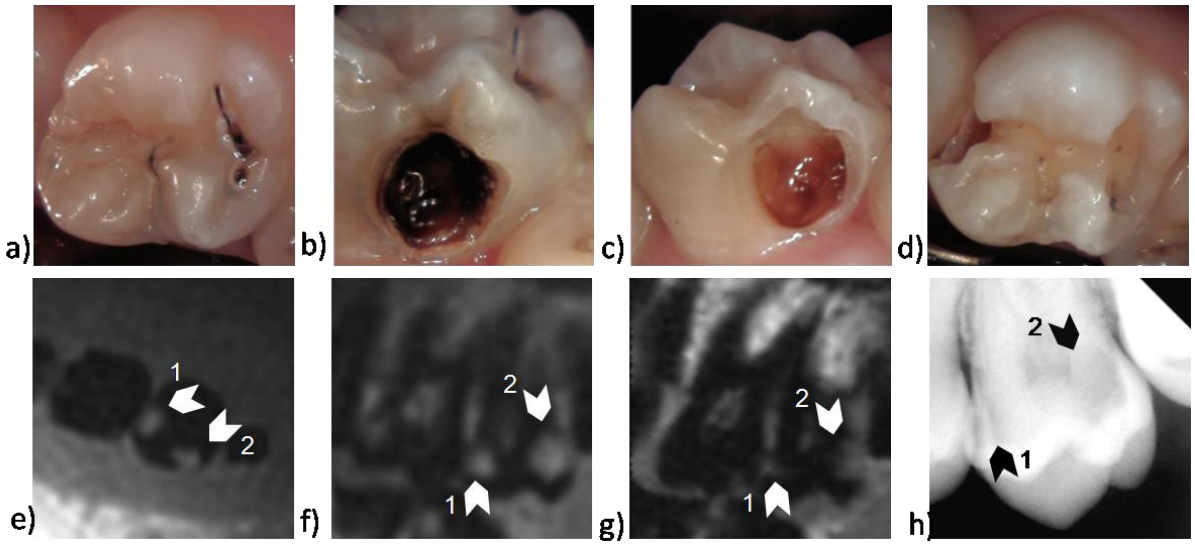


Figure 13: CI caries lesion: intra-oral pictures (a) and (b) prior to dental treatment and (c) and (d) after caries excavation and the respective (e) transversal and (f) parasagittal 3D-UTE, (g) parasagittal MS-TSE and (h) X-ray images of the tooth. Lesion positions are marked by arrows.

Case 2

In the second case the respective X-ray image only indicates a secondary caries in the mesial area beneath some sort of cavity lining while the distal area shows almost no conspicuities due to the superimposed structures of the amalgam filling (Figure 14f). Looked upon from the occlusal direction the amalgam complex seems to be made up of two separate fillings (Figure 14a) and interestingly enough two different amalgam materials must have been used as the distal part caused an artifact and therefore obstructed the MRI scans in the respective distal region of the tooth. Yet in the mesial part of the tooth, the 3D-UTE images reveal substantial loss of dentin and a lesion spreading from mesial to distal (Figure 14d). After the pictures had been taken, the tooth was sealed temporarily with cement and the patient was handed over to the students' course for further treatment. Due to the partly blurred 3D-UTE image, the qualitative assessment was not pursued any further.

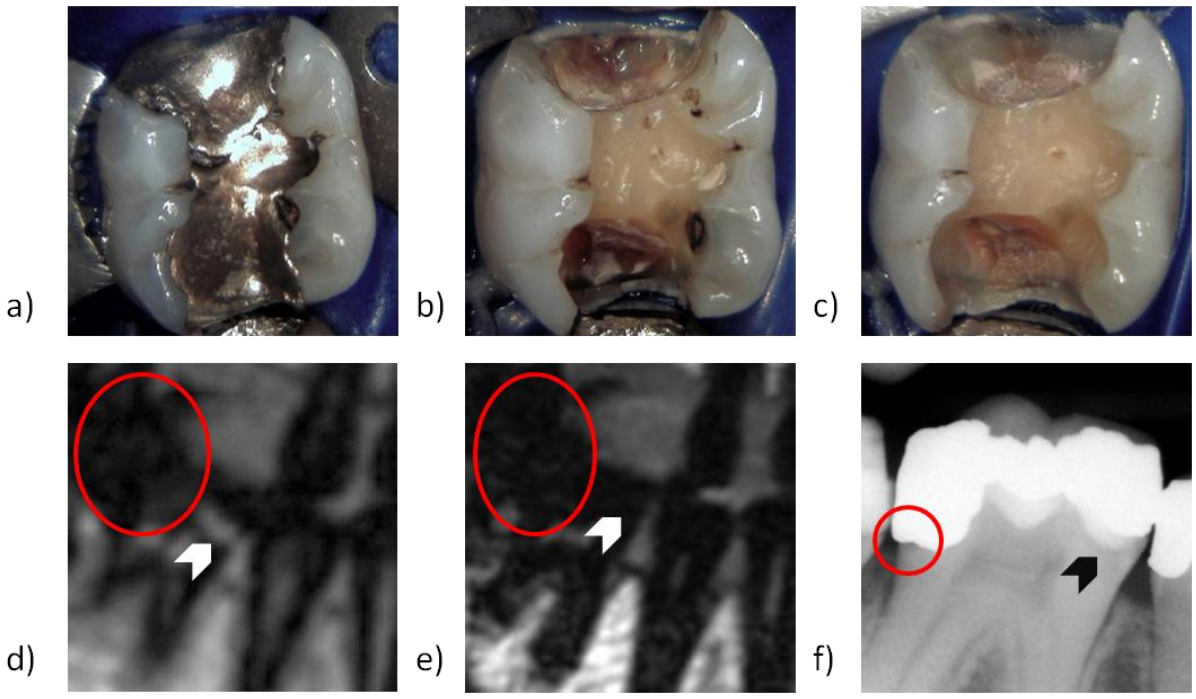


Figure 14: CII secondary caries lesion: intraoral pictures of dental treatment (a) prior to treatment, (b) after filling removal and (c) after excavation and the respective (d) UTE (e) MS-TSE and (f) X-ray images. The mesial lesion is marked by an arrow. The distal part could not be identified in the MR images due to metal artifacts (red circle).

Case 3

The third clinical case shows a seemingly intact occlusal fissure sealant and a minor conspicuous pore in the distal otherwise untouched part of the fissure (Figure 15a). However, after composite removal a small cavity right in the center of the tooth could be observed and after further excavation a huge defect was found and documented (Figure 15b and 15c). In this case the X-ray image did not provide any indication for necessary treatment.

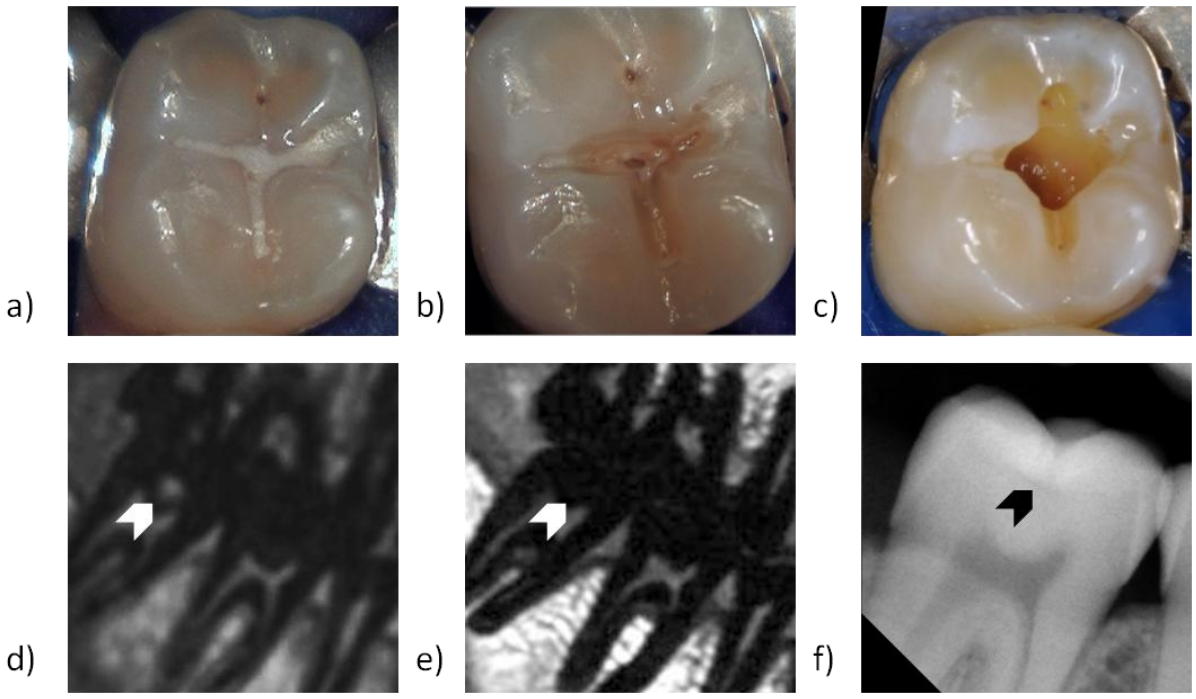


Figure 15: CII occlusal (hidden) caries under a fissure sealant: intraoral pictures of dental treatment (a) prior to treatment, (b) after fissure sealant removal and (c) after excavation and the respective (d) 3D-UTE, (e) MS-TSE and (f) X-ray images. Lesion position is marked by an arrow.

Case 4

In the fourth case a second lower molar with one buccal and one occlusal amalgam filling is presented (Figure 16a). Due to the superimposed buccal filling material the caries beneath the occlusal filling is not visible in the X-ray image (Figure 16f), although the 3D-UTE images show a bright signal. Again, the documented situation after excavation revealed a large defect (Figure 16c), proving the correct assessment by 3D-UTE (Figure 16d).

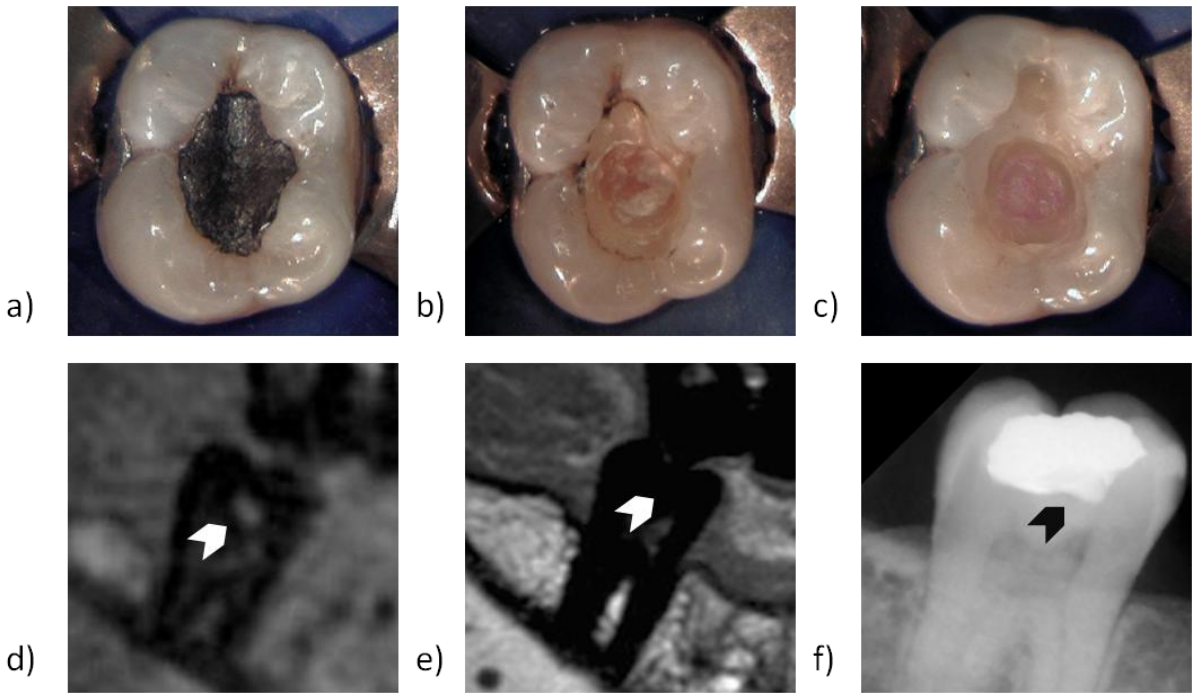


Figure 16: CIII caries: intraoral pictures of dental treatment (a) prior to treatment, (b) after filling removal and (c) after excavation and the respective (d) 3D-UTE, (e) MS-TSE and (f) X-ray images. Lesion position is marked by an arrow.

Qualitative assessment

Silicone impressions of the respective jaws were taken after excavation and plaster models were made from them. For qualitative analysis, the XR images of the plaster models were compared to the in-vivo MR and X-ray images as shown in figure 17. The shape of the lesion after excavation was estimated from the X-ray of the plaster models and transferred to the in-vivo images. The lesion extensions from the in-situ situations confirm the lesion size in the 3D-UTE images and the respective underestimation of lesion size in the XR images.

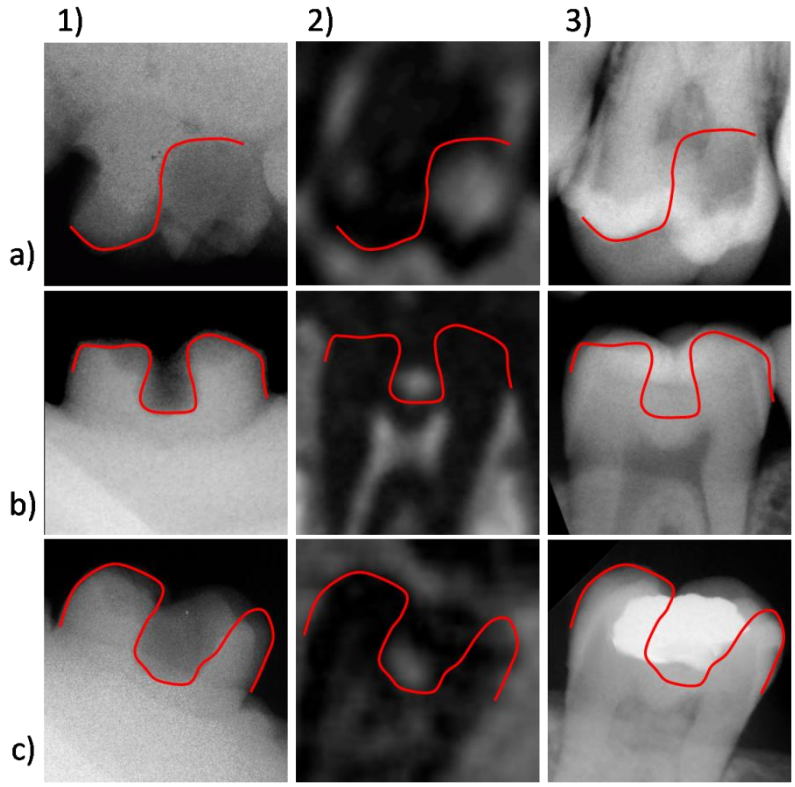


Figure 17: Qualitative analysis of the in-situ findings: comparison between (1) the X-rayed plaster models, (2) the 3D-UTE images and (3) the XR images prior to dental treatment of (a) case 1 (b) case 3 and (c) case 4.

4 Discussion

The limited performance of conventional MRI for imaging mineralized components is caused by the lack of protons and the very short spin-spin relaxation (T2) rates due to the susceptibility interfaces in the microscopic mineral structures. For the formation of a sensible MRI signal from the enamel and dentin layers, an increase of unbound water and a reduction of the random dephasing of the spins are required.

The pathogenesis of caries indicates an increase in proton density due to demineralization caused by the bacterial acid turnout. The subsurface demineralizations cause a gain in porosity of the mineral tissues and finally lead to structural collapse and necrosis. Current imaging methods applied to dental imaging rely on the increasing porosity during formation of caries lesions. Clinicians take advantage of it as well: it explains why a white-spot lesion looks white and why a dentist can estimate the depth of penetration of a caries lesion by drying the tooth surface with his multifunction syringe [28].

The observed MRI signal behavior is consistent with the process of caries development. During the initial phase, the increase of the proton concentration (acid formation / accumulation) results in a stronger local magnetization but substantial random dephasing is still inherent due to the surrounding intact crystalline microstructures. Bracher et al. showed that a decrease of the local mineralization simultaneously causes a slight decrease of the local random dephasing. As a consequence, a slight but significant increase of the local T2 relaxation time can be observed ($T2^*_{dentin}$= 324 ± 94 µs; $T2^*_{lesion}$= 649 ± 399µs) [5]. Since the resulting relaxation time is still well below 1ms, an MRI signal can only be observed with ultra-short echo time techniques. With increasing demineralization and mineral breakdown, the local magnetization and the T2 relaxation time will continue to increase, yielding a sensible MR signal even for conventional spin echo imaging techniques.

The MRI findings are supported by the observed visibility of lesions in the X-Ray images. A slight demineralization does not ensure sufficient contrast in the projective X-ray images, whereas increasing demineralization with subsequent breakdown of the mineral structure causes an increasingly sensible XR contrast.

The introduced classification most likely categorizes the caries lesions according to the degree of mineral degradation. Lesions not visible by X-ray but visible by 3D-UTE (CIII - lesions) likely indicate early demineralization with no substantial breakdown of the microscopic mineral structure. This hypothesis is supported by the significant smaller extent of C-III lesions as compared to C-I/II lesions. Pathologically, the significantly larger appearance of the lesions in 3D-UTE may indicate an initial damage of the surface zone in the proximity of the body/center of the lesion. With increasing demineralization of the dentin, the lesions become increasingly more visible in XR (CII lesions), whereas visibility of the lesions in conventional MRI (CI lesions) is not sufficient before substantial breakdown of the microscopic mineral structure. In total, CIII-lesions made up an amount of 15% and could not be detected by conventional radiography. Not all of them can be allotted to initial lesions, given that a minor proportion of the CIII lesions are not visible by XR due to superimposed structures. This could be overcome by e.g. applying DVT in cases beam hardening artifacts do not cause complete image degradation. The remaining CIII lesions, however, and the larger dimensions of all lesions as compared to the XR data support the clinical finding that the extent of a lesion is normally underestimated by X-ray and hence the accurate border of the bacterial infiltration is only insufficiently accessible. The hypothesis is well supported by the four clinically investigated patients. In all cases, the dimensions of the caries lesions were larger than the respective dimensions in the XR. Assessment of the lesion dimension after excavation clearly showed an excellent concordance between the dimensions derived from the 3D-UTE data and the dimensions derived from the imprint taken after excavation. This clearly indicates the superior performance of MRI in identification of the bacterial frontier. Especially of interest in this context may be the observed significantly reduced distance of the lesion to the pulp observed by 3D-UTE MRI when compared with XR. This may enable improved identification of pulp regions at high risk for direct pulp capping.

In a study conducted by Tymofiyeva et al. a conventional MS-TSE imaging technique with higher spatial resolution and a rather long echo time of TE = 12ms had been applied for imaging of caries lesions in vivo [68]. The authors promoted the use of a spin-echo technique due to its high robustness towards artifacts caused by dental fillings. In their attempt the patient's mouth was partly filled with contrast medium doped agarose gel to

ensure sufficient image contrast. While the resulting bright signals could be attributed to contrast medium leaking into the lesions, a direct visualization approach must be questioned. In our study only lesions with a substantial loss of the mineral structure of the tooth could be assessed by the MS-TSE imaging technique, yet inaccurate in size and with lower display quality. In this study a total of 14 teeth were not accessible neither by the two MRI imaging techniques due to severe image degradation caused by filling materials. Both techniques showed a similar artifact level and none of the 14 teeth showed superior image quality in MS-TSE. In direct comparison of the two investigated MRI techniques, there was no advantage for the MS-TSE technique neither due to the reduced metal artifact sensitivity nor the increased spatial resolution. Indeed, in direct comparison, the 3D-UTE technique was clearly more sensitive than the MS-TSE technique.

Ferromagnetic materials like nickel, cobalt and chrome are being widely used in the composition of surgical steel and in dental alloys for the fabrication of crowns, bridges or prostheses. Especially wires and fixed braces (e.g. multi-band technique or retainers) used for orthodontic treatment containing high percentages of chrome and nickel cause severe image degradation. These conductive materials produce eddy-currents and cause local field distortions resulting in image blur and signal voids in the MR images. As mentioned before, Boujraf conducted an initial feasability study to examine 17 different samples of commercially available dental materials commonly used nowadays [4]. He could show that the formation of artifacts highly depends on the imaging method used and also on the composition of the dental material. The 3D-UTE imaging technique enables extremely short echo times of TE=50µs or even less. Compared to conventional sequences this causes a significant reduction of the resulting artifact levels. Interestingly, amalgam and composite materials were most compatible with MRI and unless materials consisting of nickel, cobalt or chrome were used, no severe distortions or signal voids were observed. Since especially recent alloys contain only little or even none of the critical materials, the limitations of MRI due to image artifacts will be less of an issue in the future. In the present study only two patients had to be excluded because of severe image degradation due to ferromagnetic materials. All artifacts caused from the 14 teeth were restricted to local distortions and did not show any wide range image degradation as known from

volume CT. The limitations of 3D-UTE due to dental filling materials were less severe than expected.

An important concern about MRI results from the almost inverted contrast when compared to the image appearance of conventional DVT or XR scans. Where in dental radiographs mineralized structures appear bright and soft tissues dark, in MRI, the image contrast seems inverted. Furthermore, conventional bitewing radiographs discriminate well between the enamel and the dentin which represents the basis for today's caries classification systems, which is difficult to achieve with MRI.

Another limiting factor for the wide application of MRI is its intrinsically poor signal-to-noise ratio (SNR). Since in this study a high-field (3T) whole-body clinical MR system has been used, it will be interesting if further research and development of dedicated dental MR systems, which will be subject to immense expenditures, will meet the required SNR constraints at a cost point attractive for dental applications. Due to the limited penetration depth of the prototype carotid coil which had to be put on the cheek outside of the mouth, some signal-to-noise reductions have been observed in patients where the distance between the coil and the teeth was too large. The use of a more dedicated e.g. intraoral receiver coil could diminish the existing problems [69].

For detection of early demineralizations it would be desirable to clearly delineate the highly mineralized tissues which could not be achieved in all patients in the present study due to the limits in SNR. In the past, dentistry's approach to treating caries has been predominantly invasive while modern dentistry has evolved to a minimally invasive approach. This minimally invasive concept incorporates the concept of detecting, diagnosing, intercepting and treating dental caries on the microscopic level [51]. The focus is on maximum conservation of demineralized, non-cavitated enamel and dentin by the means of e.g. remineralization or sealing of the lesions to defer operative intervention as long as possible. It is well-recognized that it is possible to arrest and even reverse the mineral loss at an early stage. Enamel and even dentin demineralization is not a continuous, irreversible process, but must be looked upon as a series of demineralization and remineralization cycles. Invasive treatment of lesions spreading even slightly into the

dentin is not generally indicated, as caries progression through the enamel, even in active lesions, is very slow. The determination of the individual caries activity is often difficult to assess and needs longitudinal monitoring [43]. Once control of the infection is achieved the patient's caries risk status and evidences of lesion demineralization can be monitored [49, 50, 66].

The upcoming techniques address the issue of early detection signs of this disease such as minor demineralization. Here, the currently applied intra-oral XR does not provide the required sensitivity. Cone-beam computed tomography (CBCT) may perform better in the identification of initial demineralization, but according to the European Commission its application in caries detection and diagnosis is not indicated due to the related high X-ray doses and artifacts rising form filling materials [12, 61]. As 3D-UTE signals derive from acids, the detection of signals with differences in brightness could indicate acidogenic bacterial activity and could distinguish between an active or inactive caries process. Measuring the intensity and signal strength at specific spots along the infected tissues would open up the possibility of lesion monitoring. By visualizing the spreading of a lesion into the dentin a fixed point could be defined that could set the course between the different effective therapies.

Ongoing research has to prove if this new method of early caries detection will allow us to fully implement this new approach to the management of dental caries.

5 Summary

The objective of this thesis was to investigate the potential of a new magnetic resonance imaging (MRI) technique at a high-field (3Tesla) whole-body clinical system for the assessment of caries lesions and early demineralization. In an initial in-vitro study it could be shown that with adjusted imaging parameters of the ultra-short echo time (UTE) sequence a clear delineation between the different hard dental tissues at high spatial resolution and with sufficient image contrast was feasible.

In the following clinical study the aim was to investigate the transfer to patients from the clinical students' course of the Department of Conservative Dentistry and Periodontology of the University of Ulm. On the basis of two different MRI sequences for dental applications, one conventional multi-slice turbo spin-echo (MS-TSE) and one 3D ultra-short echo time (3D-UTE) sequence, the applicability for the detection of caries lesions was evaluated. The results were compared to the findings in existing conventional intra-oral X-ray images and four of the examined patients volunteered for additional in-situ documentation.

In all cases, the dimensions of the caries lesions identified by 3D-UTE MRI were significantly larger than the respective dimensions in the X-ray images. Furthermore, the lesion extensions from the in-situ documentations confirm the lesion size in the 3D-UTE images and the respective underestimation in the X-ray images. In direct comparison of the two investigated MRI techniques, there was no advantage for the MS-TSE technique at any time, yet the 3D-UTE technique showed a much higher level of sensitivity than the MS-TSE technique.

As current imaging methods applied to dental imaging rely on the increasing porosity during lesion formation, the observed 3D-UTE signal behavior is consistent with the process of caries development which is based on an increase in proton density due to demineralization. The introduced lesion classification most likely categorizes the lesion development according to the degree of early demineralization and mineral degradation.

In summary, this clinical study enabled to obtain a sensitivity of 97.5% for 3D-UTE, 85% for X-ray and 17% for MS-TSE. The limitations of 3D-UTE due to dental filling materials

were less severe than expected and unless materials consisting of nickel, cobalt or chrome were used, no severe distortions or signal voids could be observed.

Further research and development need to be continued, as it has been proven that this new radiation-free method of early caries detection represents another opportunity for the management of dental caries.

6 References

[1] Aguiar MF, Marques AP, Carvalho AC, Cavalcanti MG: Accuracy of magnetic resonance imaging compared with computed tomography for implant planning. Clin Oral Implants Res 19: 362–365 (2008)

[2] Baumann MA, Doll GM, Zick K: Stray-field imaging (STRAFI) of teeth. Oral Surg Oral Med Oral Pathol 75: 517-522 (1993)

[3] Boujraf S, Hofmann C, Ulrici J, Hell E, Haller B, Rasche V: Microstructural assessment of dental tissues by quantitative MRI using ultra-short echo times (UTE): in-vitro evaluation. In Proc Int Soc Magn Res Med Annual Meeting, Honolulu: 4518 (2009)

[4] Boujraf S, Hofmann C, Maschka R, Ulrici J, Hell E, Haller B, Rasche V: In-vitro quantification of dental filling induced artifacts in dental magnetic resonance imaging using ultra-short echo time (UTE) at 3 Tesla. In Proc Int Soc Magn Res Med Annual Meeting, Honolulu: 4520 (2009)

[5] Bracher AK, Bornstedt A, Ulrici J, Hell E, Rasche V: In vivo and in vitro T2* quantification of carious lesions by ultra-short echo time (UTE) MRI. In Int Soc Magn Res Med, Montreal 19: 4507 (2011)

[6] Bundesamt für Strahlenschutz: Positionsbestimmung des Bundesamtes für Strahlenschutz zu Grundsatzfragen des Strahlenschutzes („Leitlinien Strahlenschutz“) (2005). http://www.der-mast-muss- weg.de/pdf/appell/BfS_Leitlinien_ Strahlenschutz.pdf polling date: 18.03.2009

[7] Bundesamt für Strahlenschutz: Jahresbericht 2004 (2004). http://www.bfs.de/de/bfs/druck/jahresberichte/jb2004.html polling date: 18.03.2009

[8] Bundesministerium: Verordnung über den Schutz vor Schäden durch Röntgenstrahlen (Röntgenverordnung), Bundesgesetzblatt Jahrgang 2003, Teil I, Nr. 17, ausgegeben zu Bonn am 5. Mai 2003 (2003). http://www.aroe.org/media/user/document/downloads/roev.pdf polling date: 11.03.2009

[9] Chen YJ, Gallo LM, Meier D, Palla S: Dynamic magnetic resonance imaging technique for the study of the temporomandibular joint. J Orofac Pain 14: 65–73 (2000)

[10] Claus EB, Calvocoressi L, Bondy ML, Schildkraut JM, Wiemels JL, Wrensch M: Dental x-rays and risk of meningioma: Cancer 118: 4530-4537 (2012)

[11] Düker J: Intraorale Aufnahmen. In Düker (ed.): Praxisleitfaden Zahnärztliche Radiologie, 1. Aufl., Elsevier Urban&Fischer, München: 86-98 (2006)

[12] European Commission. Radiation protection no. 172: cone beam CT for dental and maxillofacial radiology, Evidence Based Guidelines, Luxembourg: Directorate-General for Energy Directorate D - Nuclear Energy Unit D4 - Radiation Protection (2012)

[13] Featherstone JD: Caries detection and prevention with laser energy. Dent Clin North Am 44: 955-969 (2000)

[14] Funduk N, Kydon DW, Schreiner LJ, Peemoeller H, Miljković L, Pintar MM: Composition and relaxation of the proton magnetization of human enamel and its contribution to the tooth NMR image. Magn Reson Med 1:66-75 (1984)

[15] Gray CF, Redpath TW, Smith FW, Staff RT: Advanced imaging: magnetic resonance imaging in implant dentistry: a review. Clin Oral Implants Res 14: 18–27 (2003)

[16] Gray CF, Redpath TW, Smith FW: Magnetic resonance imaging: a useful tool for evaluation of bone prior to implant surgery. Br Dent J 184: 603–607 (1998)

[17] Gruwel MLH, Latta P, Tanasiewicz M, Volotovskyy V, Sramek M, Tomanek B: MR imaging of teeth using a silent single point imaging technique. Appl Phys A 88: 763-767 (2007)

[18] Haak R, Rosenbohm J, Noack MJ, Wicht MJ: Röntgenologische Kariesdiagnostik und Therapieentscheidung. Quintessenz 58: 927-937 (2007)

[19] Haak R, Wicht MJ, Ritter L, Kusakis P, Noack M J: Cone beam tomography for the detection of approximal carious cavitations. Caries Res 40: 346 (2006)

[20] Hannigan O, O'Mullane DM, Barry D, Schafer F, Roberts AJ: A caries susceptibility classification of tooth surfaces by survival time. Caries Res 34: 103-108 (2000)

[21] Helenius LMJ, Tervahartiala P, Helenius I, Al-Sukhun J, Kivisaari L, Suuronen R, Kautiainen H, Hallikainen D, Lindqvist C, Leirisalo-Repo M: Clinical, radiographic and MRI findings of the temporomandibular joint in patients with different rheumatic diseases. Int J Oral Maxillofac Surg 35: 983–989 (2006)

[22] Hintze H, Wenzel A, Danielsen B, Nyyad B: Reliability of visual examination, fibre-optic transillumination and bitewing radiography, and reproducibility of direct visual examination following tooth separation for the identification of cavitated carious lesions in contacting approximal surfaces. Car Res 32: 204-209 (1998)

[23] Hirsch E: Digitale Volumentomographie in der Endodontie und Parodontologie. Quintessenz 58: 939-942 (2007)

[24] Holmes JE, Bydder GM: MR imaging with ultra-short TE (UTE) pulse sequence: Basic Principles. Radiography 11: 163-174 (2005)

[25] Idiyatullin D, Corum C, McIntosh A, Moeller S, Garwood M: Direct MRI of human teeth by SWIFT. In Proc ISMRM/ESMRMB Annual Meeting, Berlin, Germany 383 (2007)

[26] Idiyatullin D, Corum C, Park JY, Garwood M: Fast and quiet MRI using a swept radiofrequency. J Magn Reson 181: 342-349 (2006)

[27] Imamura H, Sato H, Matsuura T, Ishikawa M, Zeze R: A comparative study of computed tomography and magnetic resonance imaging for the detection of mandibular canals and cross-sectional areas in diagnosis prior to dental implant treatment. Clin Implant Dent Relat Res 6: 75–81 (2004)

[28] Kidd EAM, Fejerskov O: What constitutes dental caries? Histopathology of carious enamel and dentin related to the action of cariogenic biofilms. J Dent Res 83: C35-C38 (2004)

[29] Lam EW, Hannam AG, Wood WW, Fache JS, Watanabe M: Imaging orofacial tissues by magnetic resonance. Oral Surg Oral Med Oral Pathol 68: 2–8 (1989)

[30] Larson PEZ, Gurney PT, Nayak K, Gold GE, Pauly JM, Nishimura DG: Designing long-T2 suppression pulses for ultra-short echo time imaging. Magn Reson Med 56: 94-103 (2006)

[31]Lehmann KM, Hellwig E: Ätiologie der Zahnkaries. In Lehmann Hellwig (eds): Zahnärztliche Propädeutik, 10. Aufl., Elsevier Urban&Fischer, München, S.85–90 (2005)

[32] Lehmann KM, Hellwig E: Schmelzkaries. In Lehmann Hellwig (eds): Zahnärztliche Propädeutik , 10. Aufl., Elsevier Urban&Fischer, München, S.92 (2005)

[33] Lloyd CH, Scrimgeour SN, Chudek JA, Hunter G, MacKay RL: Application of magnetic resonance microimaging to the study of dental caries. Caries Res 34: 53-58 (2000)

[34] Lloyd CH, Scrimgeour SN, Chudek JA, Hunter G, MacKay RL: Magnetic resonance microimaging of carious teeth. Quintessence Int 28: 349-355 (1997)

[35] Lussi A, Megert B, Longbottom C, Reich E, Francescut P: Clinical performance of a laser fluorescence device for detection of occlusal caries lesions. Eur J Oral Sci 109: 14-9 (2001)

[36] Lussi A: Impact of including or excluding cavitated lesions when evaluating methods for the diagnosis of occlusal caries. Caries Res 30: 389-393 (1996)

[37] Lussi A, Firestone A, Schoenberg V, Hotz P, Stich H: A In vivo diagnosis of fissure caries using a new electrical resistance monitor. Caries Res 29: 81-87 (1995)

[38] Lussi A: Comparison of different methods for the diagnosis of fissure caries without cavitation. Caries Res 27: 409–416 (1993)

[39] Manfredini D, Guarda-Nardini L: Agreement between research diagnostic criteria for temporomandibular disorders and magnetic resonance diagnoses of temporomandibular disc displacement in a patient population. Int J Oral Maxillofac Surg 37: 612–616 (2008)

[40] Melcher AH, Zarb GA: Structure of carious enamel including the early lesion. Oral sciences reviews, Munksgaard, Copenhagen, 3: 100-160 (1973)

[41] Micheelis W, Schiffner U: Vierte Deutsche Mundgesundheitsstudie (DMS IV). Deutscher Ärzte-Verlag, Köln (2006). http://www.dgzmk.de/uploads/media/DMS_IV_Zusammenfassung_201002.pdf polling date: 01.02.2013

[42] Mischkowski R, Scherer P, Neugebauer J, Ritter L, Scheer M, Zöller JE: Digitale Volumentomographie: Perspektiven auch für den Generalisten? Quintessenz 58: 915-924 (2007)

[43] Murdoch-Kinch CA, McLean ME: Minimally invasive dentistry. JADA 134: 87-95 (2003)

[44] Müller-Stahl F: Karies - Korrelation quantitative lichtinduzierte Fluoreszenz, Mikrohärte und Mikroradiographie. Zahnmed Dissertation, Ludwig-Maximilians-Universität München (2006)

[45] Nasel C, Gahleitner A, Breitenseher M, Czerny C, Solar P, Imhof H: Dental MR tomography of the mandible. J Comput Assist Tomogr 22: 498–502 (1998)

[46] Olt S, Jakob PM: Contrast-enhanced dental MRI for visualization of the teeth and jaw. Magn Reson Med 52: 174-176 (2004)

[47] Orhan K, Nishiyama H, Tadashi S, Shumei M, Furukawa S: MR of 2270 TMJs: prevalence of radiographic presence of otomastoiditis in temporomandibular joint disorders. Eur J Radiol 55: 102–107 (2004)

[48] Park YS, Ahn JS, Kwon HB, Lee SP: Current status of dental caries diagnosis using cone beam computed tomography. Imaging Sci Dent 41: 43-51 (2011)

[49] Peters MC, McLean ME: Minimally invasive operative care, I. Minimal intervention and concepts of minimally invasive cavity preparations. J Adhes Dent 3: 7-16 (2001)

[50] Peters MC, McLean ME: Minimally invasive operative care, II: Contemporary techniques and materials - an overview. J Adhes Dent 3: 17-31 (2001)

[51] Pitts NB, Kidd EA: Some of the factors to be considered in the prescription and timing of bitewing radiography in the diagnosis and management of dental caries. J Dent 20: 74-84 (1992)

[51] Rainey JT: Air abrasion: an emerging standard of care in conservative operative dentistry. Dent Clin North Am 46: 185-209 (2002)

[52] Rathore S, Tyndall D, Wright J, Everett E: Ex vivo comparison of Galileos cone beam CT and intraoral radiographs in detecting occlusal caries. Dentomaxillofac Radiol 41: 489-493 (2012)

[53] Reich E: Eine neue Matrix zur Kariesklassifikation. FDI – 2011. zm 101: 3234-3236 (2011) http://www.zm-online.de/dl/1/9/1/3/ZM_22_2011.pdf polling date: 10.12.2012

[54] Ricketts DN, Kidd EA, Wilson RF: The electronic diagnosis of caries in pits and fissures: site-specific stable conductance readings or cumulative resistance readings? Caries Res 31: 119-124 (1997)

[55] Ricketts DN, Kidd EA, Beighton D: Operative and microbiological validation of visual, radiographic and electronic diagnosis of occlusal caries in non-cavitated teeth judged to be in need of operative care. Br Dent J 179: 214-220 (1995)

[56] Robson MD, Bydder GM: Clinical ultra-short echo time imaging of bone and other connective tissues. NMR Biomed 19: 765-780 (2006)

[57] Robson MD, Gatehouse PD, Bydder M, Bydder GM: Magnetic resonance: an introduction to ultra-short echo-time imaging. J Comput Assist Tomogr 27: 825-846 (2003)

[58] Rohen JW: Aufbau der Zähne. In Rohen (ed.): Anatomie für Zahnmediziner: Lehrbuch der funktionellen und topographischen Anatomie des Menschen, 3. Aufl., Schattauer, Stuttgart New York, S. 120-126 (1994)

[59] Schreiner LJ, Cameron IG, Funduk N, Miljković L, Pintar MM, Kydon DN: Proton NMR spin grouping and exchange in dentin. Biophysical Journal 59: 629-639 (1991)

[60] Schulze D, Heiland M, Thurmann H, Adam G: Radiation exposure during midfacial imaging using 4- and 16-slice computed tomography, cone beam computed tomography systems and conventional radiography. Dentomaxillofac Radiol 33: 83–86 (2004)

[61] Schulze R, Heil U, Gross D, Bruellmann DD, Dranischnikow E, Schwanecke U, Schoemer E: Artifacts in CBCT: a review. Dentomaxillofac Radiol 40: 265-273 (2011)

[62] Sener S, Akgänlü F: MRI characteristics of anterior disc displacement with and without reduction. Dentomaxillofac Radiol 33: 245–252 (2004)

[63] Tam LE, McComb D: Diagnosis of occlusal caries: Part II. Recent diagnostic technologies. J Can Dent Assoc 67: 459-463 (2001)

[64] Thylstrup A, Qvist V: Principal enamel and dentine reactions during caries progression. In Thylstrup A, Leach SA, Qvist V (eds.): Dentine and dentine reactions in the oral cavity. Oxford: IRL Press, 3-16 (1987)

[65] Tutton LM, Goddard PR: MRI of the teeth. Br J Radiol 75: 552–562 (2002)

[66] Tyas MJ, Anusavice KJ, Frencken JE, Mount GJ: Minimal intervention dentistry: a review. FDI Commission Project 1-97. Int Dent J 50: 1-12 (2000)

[67] Tymofiyeva O, Rottner K, Jakob PM, Richter EJ, Proff P: Threedimensional localization of impacted teeth using magnetic resonance imaging. Clin Oral Invest 14: 169–176 (2010)

[68] Tymofiyeva O, Boldt J, Rottner K, Schmid F, Richter EJ, Jakob PM: High-resolution 3D magnetic resonance imaging and quantification of carious lesions and dental pulp in vivo. MAGMA 22: 365-374 (2009)

[69] Tymofiyeva O, Rottner K, Gareis D, Boldt J, Schmid F, Lopez MA, Richter EJ, Jakob PM: In vivo MRI-based dental impression using an intraoral RF receiver coil. Concepts Magn Reson 33B: 244-251 (2008)

[70] Tymofiyeva O, Proff P, Richter EJ, Jakob P, Fanghänel J, Gedrange T, Rottner K: Correlation of MRT imaging with real-time axiography of TMJ clicks. Ann Anat 189: 356–361 (2007)

[71] Valizadeh S, Tavakkoli MA, Karimi Vasigh H, Azizi Z, Zarrabian T: Evaluation of Cone Beam Computed Tomography (CBCT) System: Comparison with Intraoral Periapical Radiography in Proximal Caries Detection. J Dent Res Dent Clin Dent Prospects 6: 1-5 (2012)

[72] Weerheijm KL, Gruythuysen RJ, van Amerongen WE: Prevalence of hidden caries. ASDC J Dent Child 59: 408-412 (1992)

[73] Weglarz WP, Tanasiewicz M, Kupka T, Skórka T, Sułek Z, Jasiński A: 3D MR imaging of dental cavities - an in vitro study. Solid State Nucl Magn Reson 25: 84-87 (2004)

[74] Wu Y, Chesler DA, Glimcher MJ, Garrido L, Wang J, Jiang HJ, Ackerman JL: Multinuclear solid-state three-dimensional MRI of bone and synthetic calcium phosphates. Proc Natl Acad Sci USA 96: 1574-1578 (1999)

7 Acknowledgements

I would like to express my appreciation and gratitude to all who made it possible for me to accomplish this thesis.

Huge thanks to Prof. Dr. Saïd Boujraf with whom I spent a long time preparing the samples and scanning the teeth in the early beginnings.

A big thank you to Anna-Katinka Bracher who helped me tremendously was it with the scanning of the patients or her general assistance with the computer programs. The countless hours we spent together were really nice and uncomplicated.

I would also like to thank my colleague Tobias Stegherr who showed a lot of active support during the showcase treatments of our patients.

Last but not least, I would particularly like to thank my thesis advisor Prof. Dr. Volker Rasche. His patience with me, his trust in me and his generous support will remain unforgotten. It was a pleasure to work in this open and friendly atmosphere.

8 Curriculum Vitae

Personal Details

Personal data removed for reasons of data protection

Education

Personal data removed for reasons of data protection

Studies

Personal data removed for reasons of data protection

Work Experience

Personal data removed for reasons of data protection

List of publications

Parts of the presented thesis have been published in the following journals and have been presented at the following scientific conferences.

Peer-reviewed articles

1. Bracher AK, Hofmann CP, Bornstedt A, Ulrici J, Geibel MA, Hell E, Janke F, Ulrici J, Haller B, Rasche V: Ultra-short Echo Time (UTE) MR Imaging for the Assessment of Caries Lesions. Dentomaxillofac Radiol 42: 20120321 (2013)

2. Bracher AK, Hofmann CP, Boujraf S, Ulrici J, Hell E, Spahr A, Haller B, Rasche V: Feasibility of ultra-short echo time (UTE) magnetic resonance imaging for identification of carious lesions. Magn Reson Med 66: 538-545 (2011)

Contributions to conferences

1. Bracher AK, Hofmann CP, Ulrici J, Hell E, Haller B, Rasche V: In-vivo assessment of carious lesions by MRI. Int J CARS 6 (Suppl 1): S223 (2011)

2. Bracher AK, Hofmann CP, Ulrici J, Hell E, Haller B, Rasche V: MRI for the assessment of acute parodontitis. Int J CARS 6 (Suppl 1): S225 (2011)

3. Bracher AK, Hofmann C, Bornstedt A, Hell E, Ulrici J, Haller B, Volker Rasche V: Accurate in vivo assessment of caries lesion extent by UTE MRI. In Proc Int Soc Magn Res Med Annual Meeting, Montreal 2685 (2011)

4. Boujraf S, Hofmann C, Ulrici J, Hell E, Rasche V: The visualization of the dental tissue components by quantitative MRI using ultra-short echo times (UTE). Int J Comp Ass Rad Surg 4: S197 (2009)

5. Boujraf S, Hofmann C, Ulrici J, Hell E, Haller B, Rasche V: Microstructural assessment of dental tissues by quantitative MRI using ultra-short echo times (UTE): in-vitro evaluation. In Proc Int Soc Magn Res Med Annual Meeting, Honolulu 4518 (2009)

6. Boujraf S, Hofmann C, Ulrici J, Hell E, Haller B, Rasche V: Microstructural assessment of dental tissues by quantitative MRI using ultra-short echo times (UTE): in-vivo evaluation. In Proc Int Soc Magn Res Med Annual Meeting, Honolulu 4519 (2009)

7. Boujraf S, Hofmann C, Maschka R, Ulrici J, Hell E, Haller B, Rasche V: In-vitro quantification of dental filling induced artifacts in dental magnetic resonance imaging using ultra-short echo time at 3 Tesla. In Proc Int Soc Magn Res Med Annual Meeting, Honolulu 4520 (2009)